KUNGL TEKNISKA HÖGSKOLAN
Royal Institute of Technology

IOF
Institute of Optical Research
Institutet för optisk forskning

Fabrication of periodically poled crystals from the KTP family and their applications in nonlinear optics

Håkan Karlsson

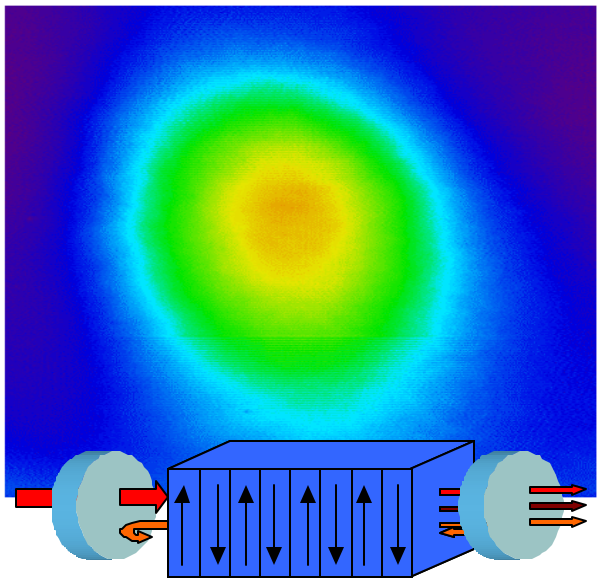

TRITA-FYS 2197 ISSN 0280-316X

Karlsson, Håkan
Fabrication of periodically poled crystals from the KTP family and their applications in nonlinear optics.
Department of Laser Physics and Quantum Optics, The Royal Institute of Technology, S-100 44 Stockholm, Sweden. TRITA-FYS 2197.

Abstract

Quasi-phasematched (QPM) nonlinear optical frequency conversion is a powerful tool in the development of new laser sources, by providing high conversion efficiency and large flexibility in terms of output wavelengths.
QPM structures are preferably implemented in bulk crystals be periodic electric field poling. Bulk crystal interactions are needed for high power generation. In this thesis, methods for achieving periodic poling in materials from the KTP family are developed. A novel technique for optical monitoring of the poling is also described. These materials combine high nonlinearity with wide transmission range, good power handling capability, and high damage thresholds. Their low coercive field also allows thick crystals to be poled into large aperture QPM devices. On the other hand, the high and varying ionic conductivity in these materials has been identified as important factor complicating the poling process.
Periodically poled QPM structures have been fabricated in flux grown KTP, RTA and RTP. Up to 3 mm thick crystals of RTA and KTP have been periodically poled, which are the thickest periodically poled crystals ever reported.
The periodically poled crystals have been used in various types of type-I QPM frequency conversion experiments, including both SHG (Second Harmonic Generation) and OPO (Optical Parametric Oscillation). Continuous wave powers exceeding 700 mW in the blue, over 65% conversion efficiency for pulsed generation of green light and up to 17 mJ pulses at 1.58 µm have been obtained. The shortest wavelength generated is 390 nm using a QPM period of 2.95 µm. The possibility of obtaining type-II QPM frequency conversion has also been demonstrated.

Keywords: quasi-phasematching, KTP, nonlinear optics, frequency conversion, periodic electric field poling, ferroelectrics, lasers, optical parametric oscillators.

Preface

Most of the work comprised in this thesis was carried out at former Institute of Optical Research (AB IOF), now Acreo AB in Stockholm, in close collaboration with the Department of Physics–Optics at The Royal Institute of Technology (KTH) also in Stockholm.

The projects have been sponsored by NUTEK, TFR, SAAB Dynamics AB (former Ericsson Microwave systems AB), The Swedish Defense Research Establishment (FOA Linköping), Celsius Tech Electronics AB, Östling Märksystem AB, Spectra Physics AB and Cobolt AB. One year of studies at Université Paris XI was supported with a grant from the Swedish Institute.

This thesis consists of an introductory part, aiming at providing a theoretical and technological background to the work, followed by reprints of the publications listed below. Periodic poling and initial optical characterisation of all the crystals used in these works were made by the author. Further optical experiments were carried out in collaboration with KTH Physics-Optics. The publications also include results from collaborations with Professor W. Sibbett's, Professor R. Wallenstein's and Professor G. Huber's groups at St. Andrews University, Kaiserslautern University and Hamburg University, respectively.

List of publications

I H. Karlsson, F. Laurell, P. Henriksson, G. Arvidsson, "Frequency doubling in periodically poled $RbTiOAsO_4$", Electron. Lett. **32**, 556 (1996)

II H. Karlsson, F Laurell, "Electric field poling of flux grown $KTiOPO_4$", Appl. Phys Lett. **71**, 3474 (1997)

III H. Karlsson, F. Laurell, "Periodic poling of $RbTiOPO_4$ for quasi-phase matched blue light generation", Appl. Phys.Lett. **74**, 1519 (1999)

IV H.Karlsson, M. Olson, G. Arvidsson, F. Laurell, U. Bäder, A. Borsutzky, R. Wallenstein, S. Wickström, M. Gustafsson, "Nanosecond optical parametric oscillator based on large-aperture periodically poled $RbTiOAsO_4$", Optics Lett. **24**, 330 (1999)*

V V. Pasiskevicius, S. Wang, J. A. Tellefsen, F. Laurell, H. Karlsson, "Efficient Nd:YAG laser doubling with periodically poled KTP", Appl. Optics **37**, 7116 (1998)

VI M. Pierrou, F. Laurell, H. Karlsson, T.Kellner, C. Czeranowsky, G. Huber, "Generation of 740 mW of blue light by intracavity frequency doubling with a first-order quasi-phase-matched $KTiOPO_4$ crystal", Optics Lett. **24**, 205 (1999)

VII S. Wang, V. Pasiskevicius, F. Laurell, H. Karlsson, "Ultraviolet generation by first-order frequency doubling in periodically poled $KTiOPO_4$", Optics Lett. **23**, 1883 (1998)

VIII G. T. Kenndy, D.T. Reid, A. Miller, M. Ebrahimzadeh, H. Karlsson, G. Arvidsson, F. Laurell, "Near-to mid-infrared picosecond optical parametric oscillator based on periodically poled $RbTiOAsO_4$", Optics Lett. **23**, 503 (1998)

IX S. Wang, V. Pasiskevicius, J. Hellström, F. Laurell, H. Karlsson, "First-order type II quasi-phase-matched UV generation in periodically poled KTP", Optics Lett. **24**, 978 (1999)

**Erratum: The temperature coefficients given in Paper IV, p 331, should be $p=[-0.7634, 2.5719, -2.3797] \times 10^{-4}$.*

Other publications by the author related to the subject, but not included in this thesis

A1 D.T. Reid, Z. Penman, M. Ebrahimzadeh, W.Sibbett, H. Karlsson, F. Laurell, "Broadly tunable infrared femtosecond optical parametric oscillator based on periodically poled $RbTiOAsO_4$", Optics Lett. **22**, 1397 (1997)

A2 T.J. Edwards, G. A. Turnbull, M. H. Dunn, M. Ebrahimzadeh, H. Karlsson, G. Arvidsson, " Continuous-wave singly resonant optical parametric oscillator based on periodically poled $RbTiOAsO_4$", Optics Lett. **23**, 837 (1998)

A3 S. I. Bozhevolnyi, J. M. Hvam, K. Pedersen, F. Laurell, H. Karlsson, T. Skettrup, M. Belmonte, "Second-harmonic imaging of ferroelectric domain walls", Appl. Phys. Lett. **73**, 1814 (1998)

A4 G. M. Gibson, G. A. Turnbull, M. Ebrahimzadeh, M. H. Dunn, H. Karlsson, G. Arvidsson, F. Laurell, "Temperature-tuned difference-frequency mixing in periodically poled $KTiOPO_4$", Appl. Phys. B **67**, 675 (1998)

A5 P. Loza-Alvarez, D. T. Reid, P. Faller, M. Ebrahimzadeh, W. Sibbett, H. Karlsson, F. Laurell, "Simultaneous femtosecond-pulse compression and second-harmonic generation in aperiodically poled $KTiOPO_4$", Optics Lett. **24**, 1071 (1999)

A6 J. Hellström, V. Pasiskevicius, F. Laurell, H. Karlsson, "Efficient nanosecond optical parametric oscillators based on periodically poled KTP emitting in the 1.8-2.5-μm region", Optics Lett. **24**, 1233 (1999)

These publications will be referred to in the text according to the notification used here.

Acknowledgements

Thanks to Dr. Fredrik Laurell, my supervisor and finally also my formal supervisor, for guidance and understanding at all kinds of levels, for always getting the point, for argues and fun.
Thanks to Prof. Klaus Biedermann, for accepting me as a PhD student, and for a lot of help and advice during the organisation of this work into a thesis.
Thanks to Dr. Jean-Michel Jonathan at Institute d'Optique and Dr. Eric Lallier at Thomson CSF/LCR in Orsay for providing me a highly enriching and by all means terrific stay in Paris by accepting me as a DEA student and project worker, respectively.
Thanks to all past and present friends and colleagues at KTH and Acreo AB (former AB IOF), especially to those directly involved in the project; Jonas Hellström, Dr. Valdas Pasiskevicius, Shunhua Wang, Rosalie Clemens, Assoc. Prof. Jens A Tellefsen, Dr. Gunnar Arvidsson, Magnus Olson, Dr. Ulf Persson and Peter Henriksson, without whom this work would have been very far away from existing. Special thanks to Jonas Hellström for good teamwork in our great sausage victory. Another special thanks to Sven Bolin, Leif Kjellberg and Rune Persson for their excellent skills in mechanics, electronics and machining. Thanks also to Prof. Walter Margulis for a lot of good advice.
Thanks to Mattias Pierrou, my roommate and closest collaborator during most of this time, for fruitful and less fruitful discussions, for a lot of help, for leaping up into the air, and for never getting rid of his old and ugly K2s.
Thanks to all our friends and colleagues in St. Andrews, Kaiserslautern, and Hamburg for strongly supporting and promoting our work. Their extensive knowledge has turned our contacts into very fruitful collaborations, and it has been a great pleasure to work with them.
Thanks to Dr. Isabelle Verrier and all the other nice people at the TSI laboratory in Saint-Etienne, for inspiring me to get into this "business".
Et enfin, merci Nadine, je ne pourrais jamais t'apporter assez de lilas!

1 Introduction – aims and motivation

Quasi-phasematched (QPM) nonlinear crystals are very attractive for use as frequency converters in laser devices due to their high nonlinearity and large flexibility in terms of output wavelengths. Combined with diode-pumped solid-state lasers, such nonlinear components allow development of compact and efficient lasers with output wavelengths ranging from the UV to the near-to-mid infrared.

Targeted applications for such lasers emitting in the visible/UV include fluorescent spectroscopy in bio-medicine, devices for printing and image recording, laser display systems and high-density optical storage. Laser radiation in the near-to mid IR is useful for molecular spectroscopy, which can be used in LIDAR based environmental monitoring, pollutant detection and process control. Other applications for infrared radiation are tissue ablation in surgery and laser-induced marking. The desired specifications on the lasers in those applications vary a lot in terms of output power, wavelength, bandwidth, pulse length, frequency stability, etc. Among other things, this puts high requirements on the flexibility and efficiency of the nonlinear components.

In quasi-phasematched frequency conversion processes, the phase shift between the interacting waves induced by the material dispersion is compensated for by an artificial wave vector in the nonlinear material. This is achieved by introducing a periodic modulation of the sign of the nonlinearity along the direction of propagation of the light. It was through the rapid development of periodic electric field poling in $LiNbO_3$, that it first became feasible to obtain efficient QPM frequency conversion in bulk devices[1]. A large number of reports on the use of Periodically Poled $LiNbO_3$ (PPLN) in nonlinear-optical experiments have since then been published[2-4], and PPLN has recently also become commercially available from two American companies.

However, certain inherent properties of PPLN limit the use of this material for short wavelength generation and in high power devices. For those applications, materials form the KTP family might provide an attractive alternative due to their high laser damage threshold, low photorefractive sensitivity, and thermal stability[5-7]. Moreover, their low coercive field and highly anisotropic structure suggest that they can be poled into large aperture QPM devices with short period gratings suitable for short wavelength generation[8].

The aim of this project was therefore to study the possibility to fabricate QPM structures in bulk materials from the KTP family by periodic electric field poling. Critical material parameters should be identified and an accordingly adapted set-up for

periodic poling should be developed. The quality of the fabricated QPM structures should be evaluated both directly by inspection and indirectly by various nonlinear-optical frequency conversion experiments. The latter should also aim at evaluating the utility of periodically poled crystals from the KTP family in practical applications.

2 $\chi^{(2)}$-nonlinear optics

2.1 Nonlinear polarisation and frequency conversion

The interaction between an electro-magnetic field and a dielectric material results in an induced polarisation field in the material. Normally, the response of the material is linear, so that several electro-magnetic waves can penetrate and propagate through the material without any interaction with each other. However, when illuminated with sufficiently intense electro-magnetic fields, the induced polarisation will exhibit nonlinear properties. That is, a series expansion of the polarisation will include higher order terms of the electromagnetic field:

$$P = e_0\left(c^{(1)}E + c^{(2)}E^2 + c^{(3)}E^3 + ...\right) = P_L + P_{NL} \qquad (2.1\text{-}1)$$

, where $P_L = e_0 c^{(1)} E$ is the linear part of the polarisation and P_{NL} the nonlinear part. ε_0 is the permittivity of free space. The value of the nonlinear susceptibility coefficients, $c^{(2,3...)}$, decays rapidly with increasing order number. This work deals exclusively with interactions based on the $c^{(2)}$ nonlinearity, which can be observed in non-centro-symmetric crystals only.

An important consequence of nonlinear properties is that several electro-magnetic waves of different frequencies can interact with each other in the material, under the condition of energy conservation. In this way, it is possible to obtain frequency conversion. There are mainly two types of frequency conversion processes. The first requires two input photons, which are added or subtracted into one photon of higher or lower energy. This type of process includes second harmonic generation (SHG), sum frequency generation (SFG) and difference frequency generation (DFG). The other type of process, parametric down-conversion, which includes Optical Parametric Oscillation (OPO), Amplification (OPA) and Generation (OPG), starts from one input photon and results in two photons of lower energies. These two generated wavelengths are referred to as signal and idler, of which the signal is the shortest. The different types of possible frequency conversion processes are illustrated in fig. 2.1-1 below.

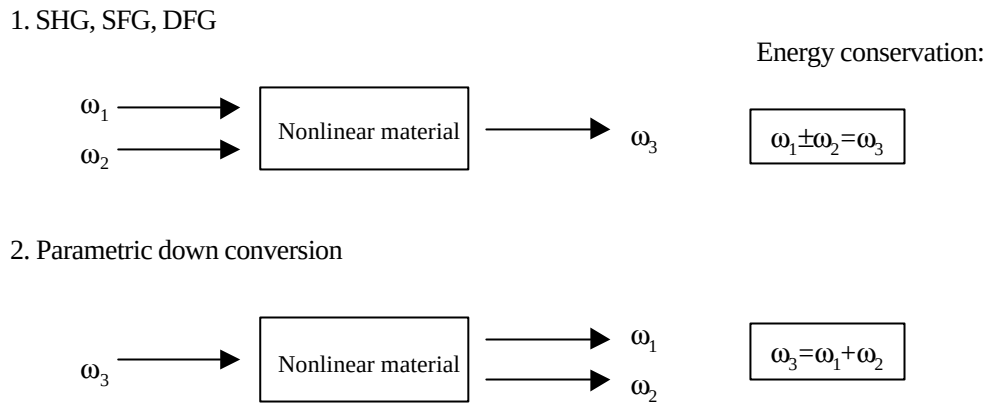

Fig. 2.1-1 Frequency conversion processes in a $c^{(2)}$-nonlinear medium.

The susceptibility coefficients, $c^{(n)}$, are tensors of rang (n+1). Thus, the components of the nonlinear part of the polarisation field in the second order can be expressed as:

$$P_i^{NL} = \sum_{j,k=1,2,3} e_0 c_{ijk} E_j E_k = e_o \sum d_{ijk} E_j E_k \qquad \text{(i=1,2,3)} \qquad (2.1\text{-}2)$$

, where $E_{j,k}$ are electric field components and where d_{ijk} is usually called the nonlinear coefficient tensor. Since E_j and E_k can be permuted without changing P_i, the d_{ijk} tensor can be transformed into a 3x6-element matrix (i.e. $d_{ijk}=d_{ikj}$) so that:

$$\begin{pmatrix} P_x \\ P_y \\ P_z \end{pmatrix}_{NL} = e_0 \begin{bmatrix} d_{11} & d_{12} & d_{13} & d_{14} & d_{15} & d_{16} \\ d_{21} & d_{22} & d_{23} & d_{24} & d_{25} & d_{26} \\ d_{31} & d_{32} & d_{33} & d_{34} & d_{35} & d_{36} \end{bmatrix} \times \begin{pmatrix} E_x^2 \\ E_y^2 \\ E_z^2 \\ 2E_y E_z \\ 2E_x E_z \\ 2E_x E_y \end{pmatrix} \qquad (2.1\text{-}3)$$

The values of the nonlinearity vary over a large range between different non-centro-symmetric crystals. However, in 1964 Miller found empirically that there is a relation between the linear and nonlinear properties in a material that yields an index (the Miller index), which remains almost constant for all materials[9]:

$$d_{ijk}^{(w_3)} = \frac{c_{ijk}^{(2)}(-w_3, w_1, w_2)}{c_{ii}^{(1)}(w_3), c_{jj}^{(1)}(w_1), c_{kk}^{(1)}(w_2)} \qquad (2.1\text{-}4)$$

By introducing the nonlinear part of the polarisation as an extra term into the standard wave equation (for waves propagating along x) it is possible to derive expressions for the coupling between the interacting waves in a nonlinear process[10]:

$$\frac{\partial^2 E}{\partial x^2} - \frac{n^2}{c^2}\frac{\partial^2 E}{\partial t^2} - \frac{s}{e_0 c^2}\frac{\partial E}{\partial t} = \frac{1}{e_0 c^2}\frac{\partial^2 P_{NL}}{\partial t^2} \qquad (2.1\text{-}5)$$

n is here the index of refraction, c the speed of light in vacuum, and σ=j/E the conductivity of the material. If considering the first type of frequency conversion process in fig. 2.1-1 and assuming two incident electro-magnetic fields at two different frequencies of the form of plane waves:

$$E_{1,2}(x,t) = \frac{1}{2}\left[E_{1,2}(x)e^{i(w_{1,2}t - k_{1,2}x)} + c.c.\right]$$

, solutions to the wave equation 2.1-5 above are obtained that include oscillating waves at the third frequency, $\omega_3=\omega_1\pm\omega_2$. Utilising the approximation of slowly varying electric field amplitude along the direction of propagation ($\frac{d^2E}{dx^2} << k\frac{dE}{dx}$) a set of three coupled differential equations for the spatial evolution of the field at each frequency component can be derived:

$$\begin{aligned}
\frac{dE_1}{dx} &= -\frac{s_1}{2n_1 e_0 c}E_1 - \frac{iw_1}{2n_1 c}d_{eff}E_3E_2^* e^{-i\Delta kx} \\
\frac{dE_2}{dx} &= -\frac{s_2}{2n_2 e_0 c}E_2 - \frac{iw_2}{2n_2 c}d_{eff}E_3E_1^* e^{-i\Delta kx} \\
\frac{dE_3}{dx} &= -\frac{s_3}{2n_3 e_0 c}E_3 - \frac{iw_3}{2n_3 c}d_{eff}E_1E_2 e^{+i\Delta kx}
\end{aligned} \qquad (2.1\text{-}6)$$

The effective nonlinear coefficient, d_{eff}, here is derived from the nonlinear matrix and depends on the polarisation direction of the incident fields. The first terms to the right are attenuation terms, which are often expressed in terms of an absorption coefficient:

$$a_m = \frac{s_m}{n_m e_0 c}.$$

Δk is the total wave vector mismatch and depends on the material dispersion, $n_m = n(w_m)$:

$$\Delta k = \frac{n_3 w_3}{c} - \frac{n_1 w_1}{c} - \frac{n_2 w_2}{c} \qquad (2.1\text{-}7)$$

The wave vector mismatch is, as shall be seen later, a key factor for the efficiency of a nonlinear process.

Integrating the last equation in 2.1-6 over x gives the value of E_3 inside the crystal at a distance, L, from the input plane (assuming the absorption to be negligible):

$$E_3(L) = -\frac{i\omega_3}{n_3 c} d_{33} E_1 E_2 L e^{-\frac{i\Delta kL}{2}} \operatorname{sinc}\left(\frac{\Delta kL}{2}\right) \qquad (2.1\text{-}8)$$

It should be noted that the expression above is valid for plane waves with perfect transversal overlap of the different beams. In the case of several input beams as in SFG, DFG and OPA it is motivated to introduce a linear dependence on the transversal overlap integral of the interacting fields. From equation 2.1-8 the generated power, P, at $l_3 = 2\pi \frac{c}{\omega_3}$ can be obtain through $I_m = \frac{1}{2} n_m \varepsilon_0 c E_m E_m^*$ and $I_m = \frac{P_m}{A}$, where A is the cross-sectional beam spot area, as:

$$P_3(L) = \frac{2\pi^2 d_{eff}^2 P_1 P_2 L^2}{n_1 n_2 n_3 l_3^2 \varepsilon_0 c A} \operatorname{sinc}^2\left(\frac{\Delta kL}{2}\right) \qquad (2.1\text{-}9)$$

An illustrative example is provided in the case of SHG, also called frequency doubling, where $\omega_1 = \omega_2 = \omega = \frac{\omega_3}{2}$. Two input photons at the same fundamental frequency are added up to generate radiation at the second harmonic frequency. With an input power P_F at the fundamental wavelength, the generated second harmonic power is given by:

$$P_{SH}(L) = \frac{8\pi^2 d_{eff}^2 P_F^2 L^2}{n_F^2 n_{SH} l_F^2 \varepsilon_0 c A} \operatorname{sinc}^2\left(\frac{\Delta kL}{2}\right) \qquad (2.1\text{-}10)$$

2.2 Phasematching

It can be noted that the generated power depends on the square of the input power and also on the square of the crystal length. The sinc^2 dependence of the generated power puts a stringent requirement on the phase matching condition, $\Delta k = 0$, for optimum conversion efficiency, as illustrated in fig. 2.2-1. The variable of the sinc^2-function is obviously affected by the length of the crystal, but also by the wavelength of the interacting waves and the temperature of the crystal through the dispersion relations. This sinc^2-curve is characteristic for most nonlinear frequency conversion processes, and is frequently reproduced in various experiments.

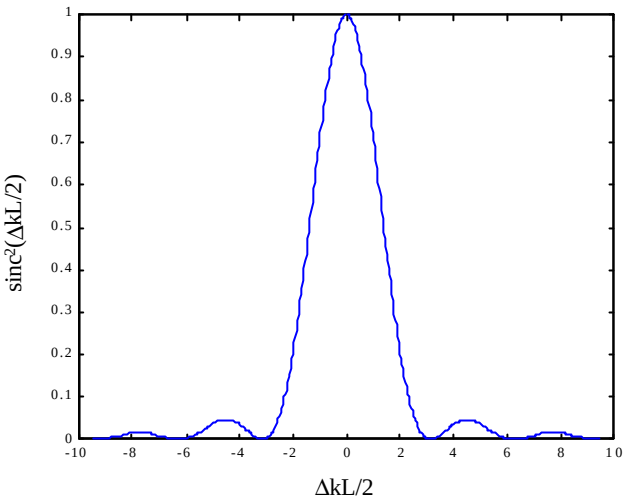

Fig. 2.2-1 Output power dependence on phasematching.

Due to material dispersion, n(λ), in eq. 2.1-7 the phasematching condition Δk=0 is normally not fulfilled. The length, L_c, inside the crystal which yields a phase-mismatch of π is called the coherence length. At this point, the second harmonic waves generated in the subsequent crystal segment will start to interfere destructively with the waves generated previously in the crystal[10].

$$L_c = \frac{2p}{\Delta k} \qquad (2.1\text{-}11)$$

For most configurations this coherence length is of the order of 1-100 μm, which severely limits the useful crystal length and, hence, the output power. One way to obtain high conversion efficiency over longer crystal lengths is to utilise anisotropic materials' birefringent properties, which yields different dispersion relations for different polarisation directions. With a suitable combination of wavelengths, polarisations and propagation directions, a phasematched configuration can be obtained for the nonlinear process. If the pair of input or output photons in the process have the same polarisation the phasematching is of type-I, otherwise of type-II.

Two examples of birefringently phasematched SHG are illustrated in fig. 2.2-2 below, where the refractive index at the fundamental wavelength for the ordinary wave equals the refractive index at the second harmonic wavelength for the extraordinary wave. In (a), where $\theta_m \neq (0^o, 90^o)$, the phasematching is critical, while (b) is an example of non-critical phasematching. In the case of critical phasematching the angle θ_m causes spatial walk-off between the interacting waves, since the Poynting vectors are perpendicular to the tangents of the refractive index ellipsoids at the crossing point. The walk-off angle is expressed as:

$$\rho = \left(\frac{n_o}{n_e}\right)^2 \tan(\theta_m) \qquad (2.1\text{-}12)$$

This angle limits the useful interaction length in the crystal, which is a particularly severe problem in the case of multiple-passes through the crystal with focused (mode-matched) beams, like in intra-cavity SHG configurations or OPO's. The maximum interaction length becomes[11]:

$$l_{\max} = \frac{w_0\sqrt{\pi}}{\rho} \qquad (2.1\text{-}13)$$

, where w_0 is the beam radius.

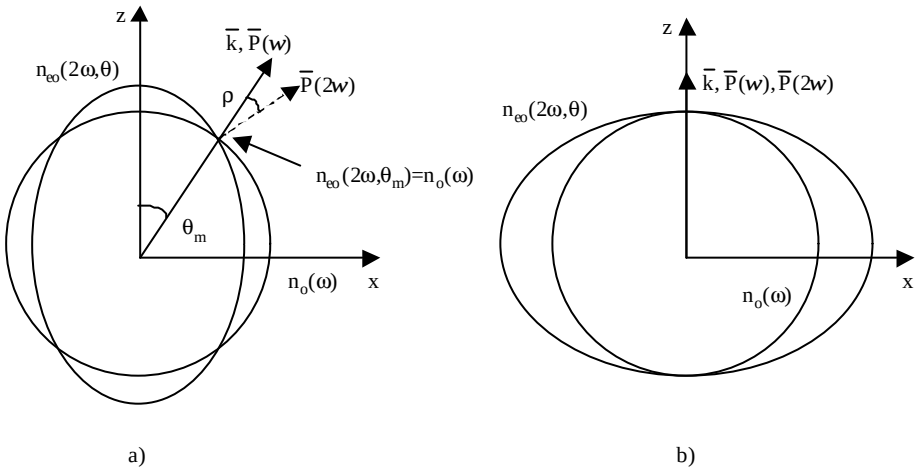

Fig. 2.2-2 Critical (a) and non-critical (b) phasematching in a uniaxial birefringent material.

The general disadvantage of birefringent phasematching is the dependence on inherent material parameters. Only a certain pair of wavelengths can be phasematched for a certain propagation direction and the range of wavelengths that can be generated from one single material is limited. Moreover, the value of the effective nonlinear coefficient depends on both the propagation direction and the polarisation directions that are used in the interaction[12].

3 Quasi-phasematching

3.1 Theoretical description

Quasi-phasematching (QPM) as a method for achieving efficient energy transfer between interacting waves in a nonlinear process was first proposed by Armstrong *et al.* in 1962[13]. In its most efficient and practical form this technique is based on a spatial modulation of the nonlinear properties along the interaction path in the material. Such a spatial modulation can be obtained in ferroelectric crystals by periodically altering the crystal orientation so that the effective nonlinearity alters between $-d_{eff}$ and $+d_{eff}$. The interacting waves still propagate with different phase velocities, but when the accumulated phase-mismatch reaches π, the sign of the driving nonlinear susceptibility is also reversed so that the phase difference is "reset" to zero. This creates a step-wise growth in the output power along the crystal length as can be seen in fig. 3.1-1. Obviously, the highest conversion efficiency is obtained when the periodicity of the modulation corresponds to $2L_c$, which represents first-order QPM, but also higher-order QPM gives continuos frequency conversion, but with lower effective nonlinearity.

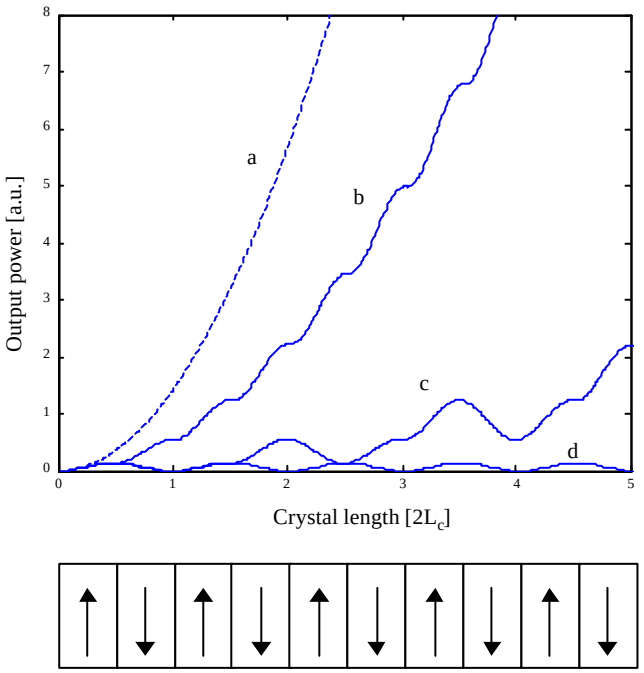

Fig. 3.1-1 Comparison of output power versus crystal length between (a) perfectly phasematched, (b) first-order QPM, (c) third-order QPM and (d) non-phasematched frequency conversion.

The introduced periodic modulation of the nonlinear coefficient can be expressed by a Fourier expansion of its spatial harmonics along the direction of propagation. This results in the following substitution into eq. 2.1-6[14]:

$$d_{eff}(x)\cdot e^{-i\Delta kx} \rightarrow d_{eff}\left[\sum_{m=-\infty}^{+\infty} c_m \cdot e^{im\frac{2p}{\Lambda}x}\right]\cdot e^{-i\Delta kx} \qquad (3.1\text{-}1)$$

,where Λ is the period of the modulation and c_m are the Fourier coefficients. Quasi-phasematching is obtained when the period is chosen such that one of the spatial harmonics $im\frac{2p}{\Lambda}x$ compensates for the phase-mismatch $-i\Delta kx$:

$$\Lambda = m\frac{2p}{\Delta k} \qquad (3.1\text{-}2)$$

For first-order QPM in the KTP materials, Λ is of the order of 2-40 µm depending on the application. The shortest periods, 2-15 µm, are needed for SHG into the UV and visible, while typical periods for OPO's in the infra-red are 15-40 µm. By assuming $d_{eff}(x)$ to be a rectangular function with a duty-cycle of $D=l/L$, where l is the length of a section over which the sign of the nonlinear coefficient remains constant (i.e $l=L/2$ yields a duty-cycle of 50%), the Fourier coefficients can be written as:

$$c_m = \frac{2}{mp}\sin(mpD) \qquad (3.1\text{-}3)$$

The value of m determines the order of QPM. Since the conversion efficiency in a nonlinear process goes as d_{eff}^2, one obtains a $1/m^2$ dependence on the order of QPM. Obviously, the largest value of c_m is $2/\pi$ and is obtained for first-order QPM with a duty-cycle of 50%. This factor $2/\pi$ explains the discrepancy between first-order QPM and birefringent phasematching in fig 3.1-1. Consequently, the nonlinear coefficient in a QPM process should be expressed as:

$$d_{eff}^{QPM} = \frac{2}{mp}d_{eff} \qquad (3.1\text{-}4)$$

3.2 Features of QPM

The use of QPM configurations in nonlinear processes has a number of advantages over conventional birefringent phasematching. Most important is the possibility to tailor the material to phasematch arbitrary processes by simply choosing an appropriate

period of the modulation according to eq. 3.1-2. This allows generation of any desired wavelengths within the transparency spectrum of the material. Moreover, phasematching can be obtained using one single polarisation along one crystal axis for all interacting waves. This yields a non-critical type-I configuration, which eliminates the problem of spatial walk-off (however, it will be shown later that also type-II QPM is feasible). Nevertheless, even QPM crystals will suffer from a type of walk-off if angle tuned. This is a wave vector walk-off rather than Poynting vector walk-off, and it can always be avoided by adjusting the crystal for propagation along the grating wave vector. Hence, in QPM crystals, temperature tuning of the wavelength is more preferred than angle tuning.

Furthermore, the use of one single polarisation together with the free choice of propagation direction gives access to the diagonal elements of the nonlinear tensor. Since, for most crystals, the d_{33} coefficient is much larger than all other coefficients, a conversion efficiency in a QPM process can be obtained that is substantially higher than in the case of birefringent phasematching. This feature has, for instance, contributed strongly to increasing the margin between gain threshold and damage threshold in OPO's, and has thereby enabled the development of new types of diode-pumped and singly resonant OPO's[15-18].

Moreover, the additional degree of freedom provided by the choice of period, can to some extent give easier access to peculiar phasematching curves. Fig. 3.2-1(a) shows the phasematched pair of signal/idler wavelengths versus pump wavelength in a QPM down conversion process for different QPM periods. In principle, the gain bandwidth of the process depends on how steep the curve is, so by altering the QPM period different phasematching characteristics for a certain fixed signal or idler wavelength can be achieved. At some point, the phasematching curves start to turn back on themselves, yielding two pairs of signal/idler. QPM periods in this range give extra-ordinary broad gain bandwidths, as illustrated in fig. 3.2-1(b). This implies that, with appropriate choice of QPM period, coherent sources of excellent continuos tunability[19] could be developed.

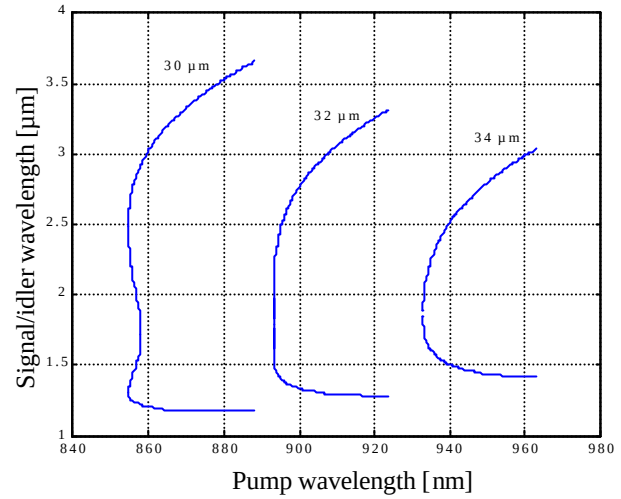

(a)

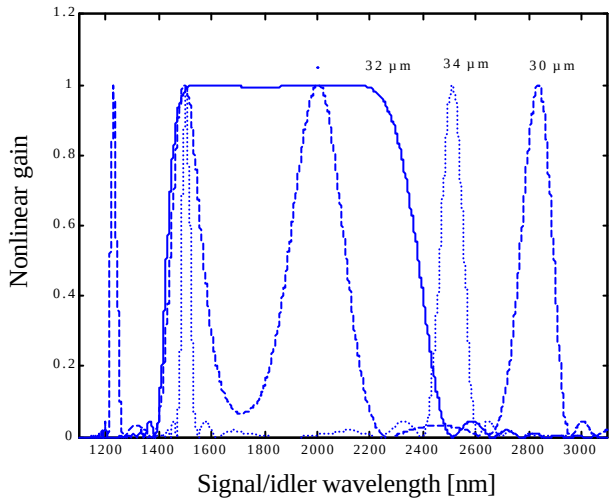

(b)

Fig. 3.2-1 (a) Phasematching characteristics (in KTP) for different QPM periods and (b) corresponding gain bandwidths (for pump at 857, 893.5 and 940 nm respectively for the QPM periods 30, 32 and 34 µm). It can be noted that a very large bandwidth is obtained for the 32 µm period and that the 30 µm period yields two pairs of signal/idler.

Finally, by introducing more sophisticated QPM structures into the material, tailored phasematching characteristics adapted to a wide range of new applications can be obtained. For instance it is feasible to achieve spatial beam shaping of the output beam by varying the conversion efficiency transversally across the interaction path[20]. Also, incorporation of several gratings into one crystal can yield multi-wavelength generation from one single crystal, either simultaneously (several gratings along interaction path) or by translation of the crystal in the beam (several grating beside each other)[15]. The former leads to the interesting possibility of obtaining extra-ordinary high pump-to-

idler conversion efficiencies in OPO's by introducing multiple gratings for subsequent signal down conversion in the cavity[21].

Moreover, the phasematched spectrum can be broadened by introducing a chirped grating. This can be used to optimise high power SHG devices by compensating for non-uniform temperature distributions along the beam caused by successively increased absorbed power of the generated second harmonic wave. Another application is temporal compression of light pulses[22,A5]. Compression is achieved by converting the low frequency components of the incoming pulse in the beginning of the crystal and the higher frequency components in the end. The group velocity dispersion in the crystal will then bring the generated components closer together in the time domain. Finally, two of those mentioned features can be combined to create a temporally separated train of compressed pulses from one single chirped pulse[23].

Fig. 3.2-2 shows an example of a gain curve from a linearly chirped QPM structure together with a non-chirped. It can be noted that the spectrum from the chirped structure is much broader, but also that the conversion efficiency is lowered.

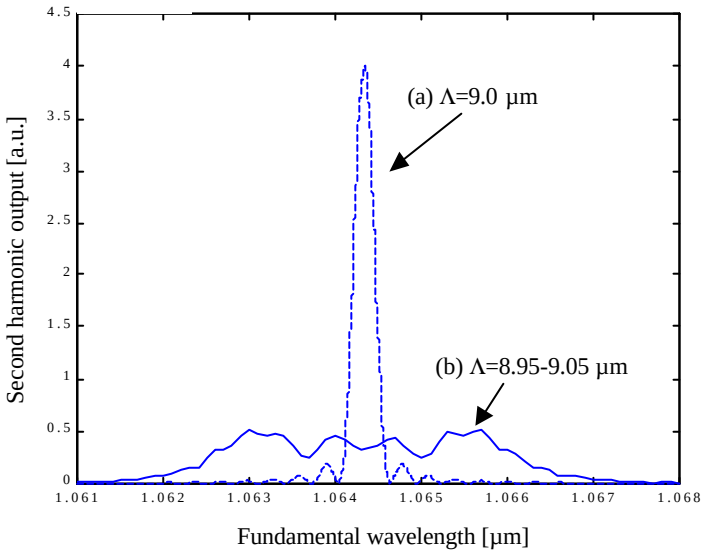

Fig. 3.2-2 Phasematching characteristics from (a) non-chirped QPM SHG compared with (b) linearly chirped QPM SHG. The crystal length is 10 mm

In principle, the most interesting feature of QPM, besides the large nonlinearity, is its flexibility, which suggests that only one or a few QPM materials should be enough to cover a large range of applications within a certain wavelength range. In this way, the search and development of new nonlinear materials can to some extent be replaced with the development of processes for fabrication of QPM structures.

3.3 Influence of defects in the QPM structure

There are various types of defects that may appear in the QPM structure, each of which affects the nonlinear conversion efficiency differently[14,24-25]. Most severe are those defects that cause an accumulated phase error, such as a constant or randomly varying period error. The acceptance in constant discrepancy from the correct period can be expressed as:

$$\frac{d\Lambda}{\Lambda} = \frac{1}{p}\left(\frac{\Lambda}{L}\right) \qquad (3.3\text{-}1)$$

, where L is the length of the crystal. For a period of 9.0 μm and a length of 10 mm, this yields an acceptance of 0.03%.

The most common defects in QPM structures fabricated by periodic poling are duty-cycle errors and missing domains. Such defects do not accumulate the phase error during propagation through the crystal and are thus less dramatic. A constant duty-cycle error reduces the conversion efficiency in the form of a cos-function for a first-order interaction, but leaves the sinc^2-feature of the spectral phasematching characteristics intact. Also in the case of missing domains there is no accumulated phase error. However, the effective interaction length is reduced and the sinc^2-curve becomes distorted. The distortion depends on the position of the areas with missing domains, but typically the side lobes grow in size and the width of the main peak is reduced and can no longer be related to the effective interaction length in the crystal. This matter is further outlined and discussed in paper I.

3.4 Implementation of QPM

The first practical demonstration of QPM was achieved by stacking thin plates of GaAs that were successively rotated by 180^o with respect to each other. Another early method was to propagate light beams in a zig-zag configuration inside a nonlinear crystal and utilise the phase shifts occurring at total internal reflection (TIR device). Despite problems with optical losses, both these two methods have recently gained new interest, the former in particular for bulk SHG of CO_2 lasers and for OPO devices generating in the far-infrared[26-27].

Other realised implementations of QPM in bulk devices include periodic modulation of the sign of the nonlinearity in ferroelectrics during growth[28] and periodic poling of ferroelectrics using an e-beam[29,30]. However, these methods often suffer from a resulting random error in period.

Shallow domain inverted QPM structures combined with waveguides have been fabricated in both $LiNbO_3$ and $LiTaO_3$ using various diffusion techniques and heat treatments[31-34]. Similar structures have been obtained in KTP by periodic in-diffusion of Rb^+/Ba^{2+}, which creates domain-inverted regions and a segmented waveguide at the same time[35-36]. The use of lithography techniques for the QPM structure fabrication eliminates the problem with random period errors. Moreover, the nice confinement of the interacting beams in waveguide interactions provides good overlap and high intensity over long interaction lengths, which yields conversion efficiencies that are one to two orders of magnitude higher than for bulk interactions, where the optimum overlap areas are determined by diffraction. More than 100 mW of blue light generation with conversion efficiencies exceeding 500%/Wcm^2 have been achieved by SHG of diode lasers in such waveguide QPM structures in KTP[36]. However, several problems including heating, optical damage and mode-coupling difficulties have so far inhibited further up-scaling of the output powers, Furthermore, manufacturing of efficient and stable QPM-waveguide devices puts though requirements on the waveguide fabrication process and the optical in-coupling.

For high power devices it is necessary to use bulk interactions. The most efficient method for fabrication of QPM structures in bulk crystals has turned out to be periodic electric field poling of ferroelectric crystals[37]. The technique consists of applying electric pulses of an amplitude exceeding the crystal's coercive field to periodic electrodes patterned on the c-faces of the crystal. The technique combines the advantages of using lithography for the design of the gratings with the possibility to form parallel domains through a bulk-like crystal thickness. Periodic poling in bulk crystals was first demonstrated in $LiNbO_3$ by Yamada *et al.* in 1993[1], and periodically poled $LiNbO_3$ (PPLN) has since then through a quick development by Webjörn[2], Myers[3], Miller[38] and others been turned into a mature nonlinear material for up to 1 mm crystal thickness. As is shown in this work, periodic poling can also be applied to materials from the KTP family, and some advantageous properties make such QPM crystals an interesting alternative to PPLN for certain applications.

4 General properties of materials from the KTP family

4.1 Introduction

KTP is a non-centro-symmetric crystalline material, which, since it was first developed in the end of the 70:ies by Bierlein and Geir, has been widely used in various nonlinear-optical applications, in particular in SHG and OPO devices based on pumping with 1 μm radiation from Nd lasers. This is due to a highly attractive combination of material properties including large nonlinearity, high damage threshold, large birefringent phasematching acceptance in angle and temperature, wide transmission, and good thermal and mechanical stability[5-6]. KTP and some of its isomorphs are available from several vendors and are today frequently used in commercial laser devices.

4.2 Structure and growth

The isomorphic KTP family compounds are characterised by the formula unit $MTiOXO_4$, where M can be K, Rb or Cs and X can be P or As[5]. Available family members are KTP, RTP, RTA, KTA and CTA. All these materials are orthorhombic and belong to the acentric point group mm2, with only slightly different lattice parameters. The structure is characterised by chains of TiO_6 octahedra, which are linked at two corners and separated by XO_4 tetrahedra. Alternating long and short Ti-O bonds occur along these chains, which result in a net z-directed polarisation and are the major contribution to the materials' nonlinear and electro-optic coefficients. These bonds are also responsible for the ferroelectric properties of the materials. The M-ion is weakly bonded to the Ti octahedra and the X tetrahedra. Channels exist in the crystal lattice along the z-axis whereby M-ions can move through a vacancy mechanism with diffusion constants several orders of magnitude larger than in the x-y plane.

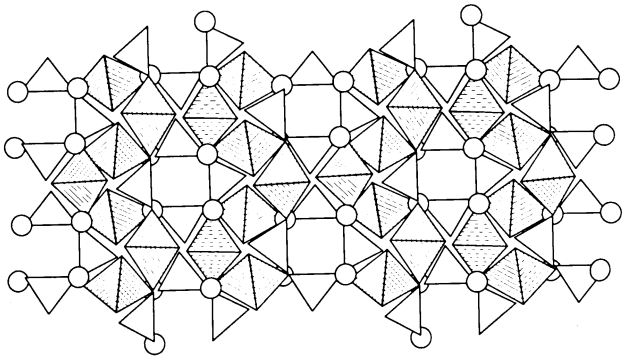

Fig. 4.2-1 Structure of KTP in x-y projection, which reveals the existence of channels along the z-axis. Shaded elements are Ti octahedra, open elements are P tetrahedra and open circles are K ions[5].

Most members of the KTP family can be grown using a high temperature solution growth process in which the material crystallises out of a molten self-flux composition when cooled[39,40]. The flux growth operates at atmospheric pressure and can yield large crystals. Self-flux means that the solvent contains no other elements than those of the final crystalline material. The growth temperature is typically 850-950 ^{o}C, and the growth time is about 5-8 weeks. In order to obtain uniform crystals free from growth striations it is necessary to minimise temperature gradients in the flux, which requires high levels of temperature control.

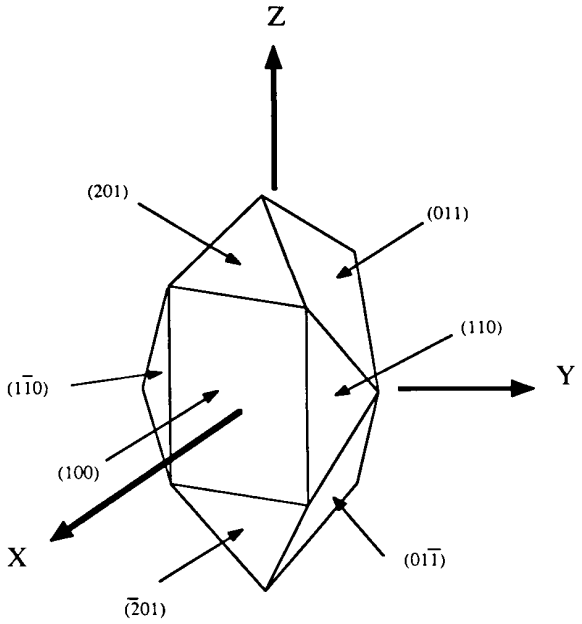

Fig. 4.2-2 Natural KTP crystal morphology[5].

KTP can also be grown by the hydrothermal technique (Ht-KTP), in which the crystals are grown at constant high pressure and lower temperature[41]. This technique yields crystals of very good uniformity and optical quality. However, the process is more complicated and takes longer time, thereby increasing the price and limiting the availability of such crystals.

4.3 Ferro-electric properties

As mentioned earlier, the main contribution to the KTP material's ferroelectric properties is provided by the long and short Ti-O bonds in the crystal lattice. This renders the KTP materials uniaxial ferroelectrics with a spontaneous polarisation along the z-direction.

Fundamental for ferroelectrics is that the spontaneous polarisation exhibits a hysteresis more or less symmetric around origo when plotted versus an applied external electric field. The spontaneous polarisation sets up an internal depolarisation field in the crystal and domain reversal is obtained if an external field exceeding this internal field is applied. This critical field, where so-called electric field poling occurs, is called the coercive field, E_c. The spontaneous polarisation, P_s, can be defined by the amount of charge, Q, it takes to reverse a single domain crystal of a certain area, A[42]:

$$Q = \int I_{pol} dt = 2 \cdot A \cdot P_s \qquad (4.2\text{-}1)$$

I_{pol} is here the charge transfer current during poling. Measurements of P_s for KTP (Ht-KTP) carried out in this work resulted in a value of 0.14 C/m^2. We have observed slight variations in the value of the coercive field not only for the different isomorphs of KTP but also within the same material, depending on supplier and quality. The variations can probably be attributed to differences in vacancy, impurity and doping levels. For the tested materials KTP, RTA and RTP the values ranges from 2.0-4.0 kV/mm, with the smallest values in general for KTP and the largest for RTP.

In order for the crystals to be useful in practical nonlinear-optical or electro-optic applications they should have a single-domain structure. It has been observed that the phosphates within the KTP family are easier to grow single domain than the Arsenates[39]. However, through advanced growth methods it is possible to generate single-domain crystals also for RTA and KTA. In the case of multi-domain formation, the lattice structure of the materials is such that domain walls parallel to the y-z plane are most probable, since formation of those is energetically favourable[43].

The anisotropic structure of the crystal lattice results in a much higher domain wall velocity for walls in the x-y plane than for walls in planes parallel to the z-axis. This is a favourable feature since it limits domain broadening when fabricating periodically poled structures along the z-axis.

Like all ferroelectric crystals the KTP materials are piezoelectric, meaning that the spontaneous polarisation is sensitive to pressure. They also exhibit pyroelectric properties, i.e. the spontaneous polarisation changes with temperature[8].

4.4 Conductivity

The dielectric properties of the KTP materials are, like for many other ion-covalent crystals, typical for ion conductors[44-45]. The M-ions are loosely bound in the lattice and can move in channel-like structures by a hopping mechanism via vacancies. These channels cause the dielectric properties to be strongly anisotropic with a conductivity along the z-axis several orders of magnitude larger than in the x-y plane. The ion hopping rate and, hence, the conductivity, s , is thermally activated with an activation energy, E_a. This can be expressed by the Arrhenius formula:

$$s = \frac{s_0}{T} e^{\left(-E_a/kT\right)} \qquad (4.3\text{-}1)$$

, where k is the Boltzmann constant and T is the temperature.

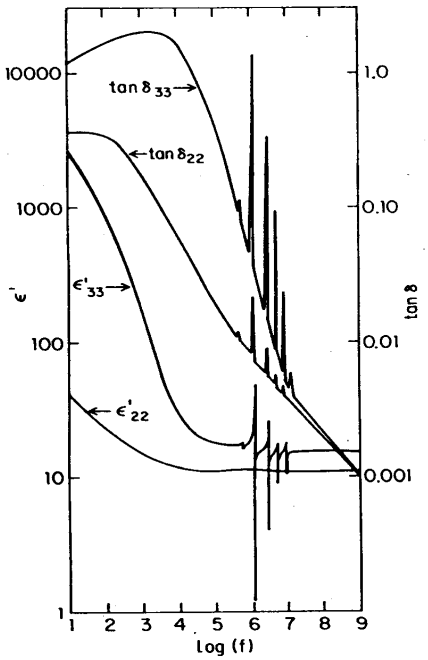

Fig. 4.3-1 Frequency dependence of the dielectric constants e_{22} (similar to e_{11}) and e_{33} in KTP[43].

The dielectric constants follow the general Debye form with e_{33} exhibiting strong low-frequency enhancement, which confirms the ion-hopping mechanism involved in the conductivity.

Unlike most other material properties of these crystals, the conductivity varies strongly between the different isomorphs. The larger Rb-ion has a much lower mobility in the lattice than the K-ions, yielding a conductivity 3-4 orders of magnitude lower in RTP and RTA than in KTP and KTA[39]. Moreover, the conductivity is very sensitive to crystal growth and impurity levels. Hydrothermally grown KTP crystals have a very low level of vacancies, probably due to lower growth temperature, and has therefore a

conductivity lower by several orders of magnitude than flux grown KTP. The dependence on impurity levels tends to cause variations in conductivity even in crystals from the same supplier.

4.5 Optical properties

Optical transmission characteristics for the KTP, RTA and RTP materials used in this work are presented in fig. 4.4-1[46]. The transmission data are taken for propagation along the x-axis with a z-directed polarisation. The characteristics were similar for other polarisation directions but some differences were observed for different propagation directions. However, the propagation direction in the optical applications presented in this work is exclusively along the x-axis.

The absorption bands at 2.8 µm most likely represent OH stretching bands, which indicates that H_2O has been incorporated in the lattice during growth. The decrease in transmission in the infrared is due to molecular absorption bands (PO_4, AsO_4 and TiO_6). Obviously, the Arsenates have an extended transmission in the infrared, which renders RTA the preferred material for applications in the 3-5 µm spectral range. In fig. 4.4-1 RTA also has a somewhat shorter cut-off wavelength in the UV. For all materials the residual absorption below 2 µm can be smaller than 1%/cm, although enhanced residual absorption has been observed for crystals with high impurity levels.

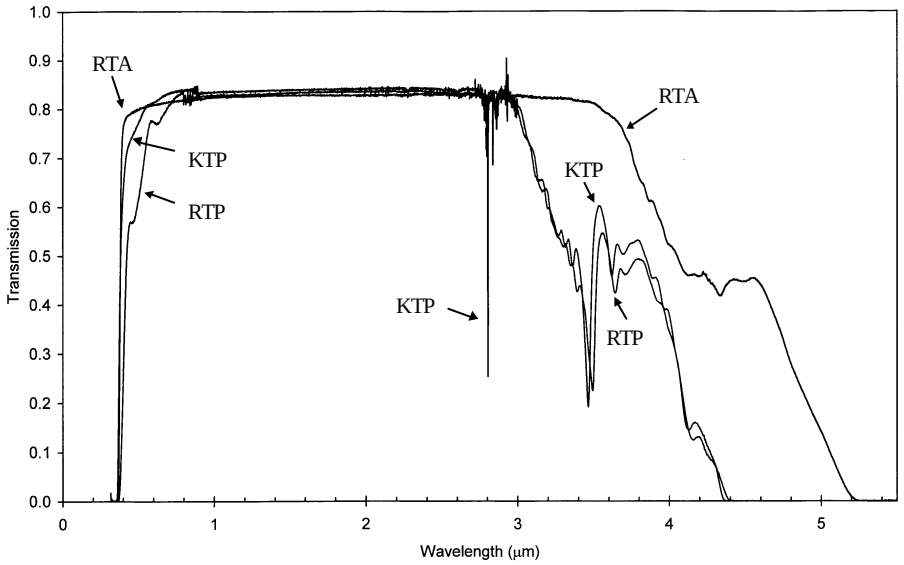

Fig. 4.4-1 Transmission characteristics for KTP, RTA and RTP used in this work. Data are taken for propagation along the x-axis (10 mm crystal length for KTP and RTA, 11.2 mm for RTP) and with linearly polarised light along the z-direction[46]. The Fresnel losses at the surfaces have not been compensated for in this plot.

There are several dispersion data for the KTP materials available in the literature, in the form of Sellmeier equations[47-51]. They all have in common to be more or less inaccurate in the infrared (>1μm), where the refractive index curve is almost flat. This is a severe problem, since it prevents correct prediction of suitable QPM periods in this wavelength range. The problem has been particularly pronounced for KTP. However, recently Fradkin *et al.* published a Sellmeier equation with an extra pole, which enables prediction of QPM periods in the infrared with decent accuracy[52]. Table 4.4-1 shows the dispersion data that most frequently have been used in this work. For QPM SHG with both interacting waves below 1 μm, these data gives an accuracy of better than± 0.5 nm in the fundamental wavelength that will be phasematched for a certain QPM period.

Sellmeier equation (λ in μm): $n^2 = A + \frac{B}{1 - C/l^2} + \frac{E}{1 - F/l^2} - D \cdot l^2$

Crystal	**Index**	**A**	**B**	**C**	**D**	**E**	**F**
KTP <1 μm Fan[47]	n_z	2.25411	1.06543	0.05486	0.02140	0 0	0 0
KTP >1 μm Fradkin[52]	n_z	2.12725	1.18431	5.14852* 10^{-2}	9.68956* 10^{-3}	0.6603	100.00507
RTA Fenimore[50]	n_z	2.18962	1.30103	0.22809	0.01390	0	0
RTP[51]	n_z	2.77339	0.63961	0.08151	0.02237	0	0

Table 4.4-1 Selected dispersion data.

The following temperature dependence of the refractive index have been used for calculations of temperature tuning characteristics in KTP and RTA:

$\frac{dn_z}{dT} = \frac{a}{l^3} + \frac{b}{l^2} + \frac{c}{l} + d$ (λ in μm)

	a (*10^6)	b (*10^6)	c (*10^6)	d (*10^6)	Thermal expansion coeff, α_1 [/^{o}C][5,PaperIV]
KTP Wiechmann[53]	12.415	-44.414	59.129	(-12.101)	11*10^{-6}
RTA Karlsson[PaperIV]	-76.34	257.19	-237.97		15.1*10^{-6}

Table 4.4-2 Temperature dependence of the refractive index in KTP and RTA. The d-coefficient is actually not needed for deriving tuning characteristics.

The coefficients for RTA were derived from OPO tuning characteristics in paper IV, and should be valid in the 1-3 μm range. No temperature tuning characteristics of RTP have been studied in this work.

The crystal symmetry of the KTP materials results in the following nonlinear and electro-optical matrices:

$$[d]=\begin{pmatrix} 0 & 0 & 0 & 0 & d_{15} & 0 \\ 0 & 0 & 0 & d_{24} & 0 & 0 \\ d_{31} & d_{32} & d_{33} & 0 & 0 & 0 \end{pmatrix} \qquad [r]=\begin{pmatrix} 0 & 0 & r_{13} \\ 0 & 0 & r_{23} \\ 0 & 0 & r_{33} \\ 0 & r_{42} & 0 \\ r_{51} & 0 & 0 \\ 0 & 0 & 0 \end{pmatrix}$$

Nonlinear susceptibility @1064 nm [pm/V][39]					Electro-optic coefficient @ 633 nm [pm/V][5]				
d_{31}	d_{32}	d_{33}	d_{24}	d_{15}	r_{13}	r_{23}	r_{33}	r_{42}	r_{51}
2.5	4.4	16.9	7.6	6.1	9.5	15.7	36.6	9.3	7.3

Table 4.4-3 Nonlinear susceptibilities and electro-optic coefficients of KTP.

It should be noted that the values of those coefficients given in the literature vary somewhat. The values are similar for all the isomorphs. Obviously, according to eq. 3.1-4, a $\left(2/\pi \cdot 16.9/7.6\right)^2 = 2$-fold increase in conversion efficiency can be obtained by attaining the d_{33} coefficient in a first-order QPM configuration compared with using d_{24} in a birefringently phasematched process.

4.6 Comparison of material properties between KTP materials and $LiNbO_3$

	KTP Flux	**KTP HT**	**RTA**	**RTP**	**KTA**	**$LiNbO_3$**
Conductivity σ_{33} [S/cm]	10^{-6}-10^{-7}	$<10^{-10}$	10^{-8}-10^{-9}	~10^{-9}	>10^{-6}	~10^{-18}
Coercive field E_c [kV/mm for 1 mm]	2.0-2.1	~2.0	2.1-2.3	2.5-4.0	~2.0	~20.7
Nonlinearity d_{33} [pm/V]	16.9	~16.9	15.8	17.1	16.2	27.0
Transparency [μm]	0.35-4.3	0.35-4.3	0.35-5.3	0.35-4.3	0.35-5.3	0.35-5.5
Phase transition [^{o}C]	946	946	792		872	1200

Table 4.5-1 Comparison of selected material parameters between the KTP isomorphs and $LiNbO_3$.

The most apparent advantage of using KTP materials for periodic poling instead of $LiNbO_3$ is the about ten times lower coercive field. While PPLN currently is limited by the high coercive field to approximately 1 mm thickness, it feasible to periodically pole several millimetres thick samples of KTP materials into large aperture QPM devices suitable for high power generation[PaperIV]. There have been some attempts to circumvent the problem of limited thickness for PPLN by diffusion bonding several plates of PPLN on the top of each other[54]. However, this is a fairly complicated process and the final device tends to suffer from losses and scattering at the interfaces. Moreover, the limited domain broadening in the KTP materials due to their anisotropic lattice structure allows fabrication of short grating periods needed for short wavelength generation[PaperVIII].

Other important features of the KTP materials are their high resistance to optical damage and their low sensitivity to photorefractive effects (see further section 6.5). The latter forces PPLN to be operated at elevated temperatures (>100 ^oC)[15], while the KTP materials can be kept at room temperature. Furthermore, the KTP materials are much less sensitive to thermal loading than $LiNbO_3$, which allows stable operation even at high average power levels and increases tolerances to absorption. The thermal instabilities in PPLN have turned out to be a severe problem in high power applications[55].

On the other hand, PPLN offers significantly higher nonlinearity ($2/p \cdot 27$) and has better transmission in the infrared (somewhat better than RTA). Generation of >6 μm radiation from short-pulsed OPO's based on PPLN has been reported[56-57] (this indicates also that generation of wavelengths somewhat longer than the cut-off wavelengths for the KTP materials given in table 4.5-1 above should be possible). Moreover, fabrication of 0.5 μm thick PPLN with periods suitable for OPO applications in the infrared is a very mature process.

By generalising, one can speculate that PPLN is most suitable for low threshold and low-to-medium output power OPO devices in the infra-red, while PPKTP materials would be more interesting for high power applications in the visible to the near-infrared. Other interesting alternatives to $LiNbO_3$ for periodic poling are $LiTaO_3$ (slightly lower coercive field, better resistance to photorefractive effects), stoichiometric $LiNbO_3$ (lower coercive field, possibly lower sensitivity to photorefractive effects)[58] and MgO:$LiNbO_3$ (lower coercive field, lower sensitivity to photorefractive effects, higher damage threshold)[59]. However, the two latter materials suffer from lack of maturity as compared to $LiNbO_3$.

Among the KTP isomorphs, Ht-KTP[60-61], RTA[PaperI,IV,VIII,62] and RTP[PaperIII] appear most attractive for periodic poling due to their lower conductivity. KTA, which has the highest conductivity, was never studied in this work. Taking the transmission

properties into consideration leaves RTA as the preferred choice of material for applications in the infrared, while Ht-KTP is known to have the best optical properties in the visible. The main reason for studying also flux grown KTP is the limited availability of the other isomorphs and Ht-KTP. At the time of this work, RTA was only available from one supplier, Crystal Associates, USA, and suffered from variations in quality in terms of homogeneity and conductivity. Ht-KTP was merely available from Litton Airtron, USA, but only in small sizes, and RTP was only available as research samples from DuPont, USA. Instead, flux grown KTP was commercially available in large size (>30 x 30 mm) wafers from several vendors in Europe, USA and China. Also, flux grown KTP was by far the cheapest alternative among the KTP materials (yet more than ten times more expensive than $LiNbO_3$). To the largest extent, the KTP material used in this work comes from China.

5 Periodic poling of KTP materials

5.1 Introduction

Periodic electric field poling of ferroelectric materials consists of applying an electric field exceeding the coercive field over periodic electrodes defined on the crystal surface[37]. This creates a regular multi-domain structure in the material. The challenge of fabricating high quality QPM structures in the material by electric field poling lies in achieving few micrometers wide domains in crystals of several millimetres in thickness. This put high demands on the poling process.

Periodic poling of $LiNbO_3$ has been studied in detail by Myers[3] and Miller[38], among others. Their works show that the domain formation can be broken up into four distinct regimes; nucleation, tip propagation, domain wall propagation and stabilisation. Nucleation of microscopic domains occurs at electric fields exceeding the coercive field, mainly at the crystal polar faces, but possibly also in the bulk. The nucleation density depends of course on the amplitude of the electric field, but also on the type of electrode[63]. The tips of the nucleated domains then propagate rapidly towards the opposite face. Thereafter, the domain walls start to propagate in the x-y plane with a velocity, that was found in $LiNbO_3$ to depend on the applied field as the sum of two exponential functions[38]:

$$v(E) = \Phi(E - E_1)v_1 e^{-d_1 / \left(\frac{E}{E_1} - 1\right)} + \Phi(E - E_2)v_2 e^{-d_2 / \left(\frac{E}{E_2} - 1\right)} \qquad (5.1\text{-}1)$$

E_1 and E_2 are field constants, both below the coercive field, v_1 and v_2 are velocity constants while δ_1 and δ_2 are dimensionless. This yields an exponentially growing function with a knee-like feature slightly above the coercive field in a logarithmic plot. It was shown that optimum control of the domain wall propagation was obtained at poling fields close to this knee.

The geometrical structure of the periodic electrode results in very high fringing fields in the transversal field component close to the surface[38]. In $LiNbO_3$ these fringing fields cause significant domain broadening under the electrically insulated areas on the surface, which reduces the quality of the resulting QPM structure. However, this problem could be circumvented by defining electrodes with a duty-cycle smaller than 50 %, and utilising the fact that domain spreading under the insulator is at some point inhibited by charges deposited by the depolarising field at the insulator-substrate interface. In KTP materials it is likely that domain wall propagation in the x-y plane is

strongly limited by the anisotropic lattice structure. This would facilitate fabrication of short period domain inverted structures of 50 % duty-cycle in thick crystals.

5.2 Influence of the conductivity

The high ionic conductivity was at an early stage identified as a key-factor that provided the main difficulty associated with periodic poling of materials from the KTP family. High ionic conductivity results in a large current flow through the crystal when the high voltage is applied.

We have observed high-voltage regimes (pulsed DC, liquid electrodes) where the conductivity exhibits non-Ohmic behaviours with rapidly decreasing resistance when the voltage is further increased. Non-Ohmic regimes have also been found for lower voltages (DC mode, metal electrodes) in KTP, but with an increasing resistivity versus voltage and time[64]. This behaviour has been explained by an enrichment of K^+ ions at the cathode, which reduces the number of vacancies and, hence, lowers the conductivity in that area. The increasing conductivity at higher voltages that we have observed is probably an avalanche effect caused by the ion migration, which leads to dielectric breakdown in the crystal for sufficiently high voltages. For certain values of the conductivity, dielectric breakdown occurs before the coercive field has been reached and, hence, poling of such crystals is inhibited. These problems were frequently observed in flux grown KTP and also in some wafers of RTA, but never in RTP.

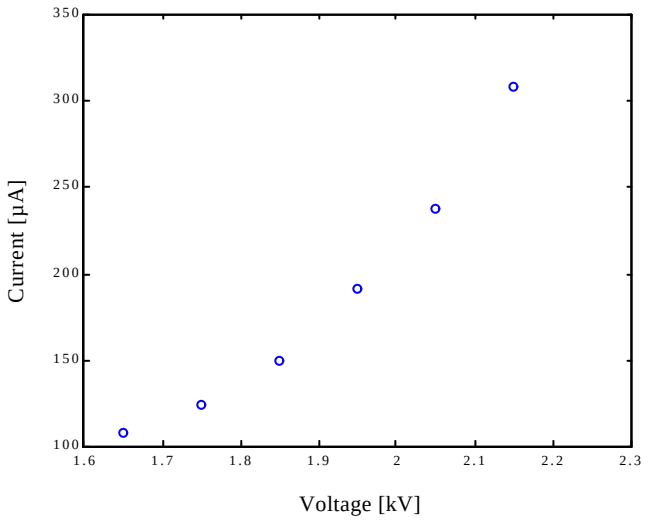

Fig. 5.2-1 Nonlinear conductivity in KTP (the voltage was applied in 6 ms long pulses).

It was found that the use of a metal film (Al, 1000-3000 Å) as one of the electrodes could decrease the conductivity with up to 4 times, as compared with using liquid

electrodes on both sides (c^+/c^-). Similar effects were obtained whether the film was applied on the c^+-face or the c^--face, and no further decrease in conductivity was obtained if metal films were applied on both sides. Obviously, the ion migration, both into and out of the crystal, is partly blocked by a metal film. On the other hand, it has been reported that in KTP some of the K^+ ions may move out of the crystal and form K_2O, which in contact with water vapour turns into KOH. The latter reacts with the metal electrode and destroys it[64].

Furthermore, we have found that the conductivity shows strong time dependence when high fields are applied, with increasing conductivity versus time. The ion migration also seems to cause thermal effects inside the crystal. The time scales varies with applied DC voltage. This led us to use short voltage pulses in order to stabilise the poling conditions. It was found that most materials exhibited a temporally stable conductivity over time-scales of the order of a few ms when fields close to the coercive fields were applied.

5.3 Poling set-up

The set-up that has been used for poling experiments in this work is quite simple. A schematic illustration is given in fig. 5.3-1.

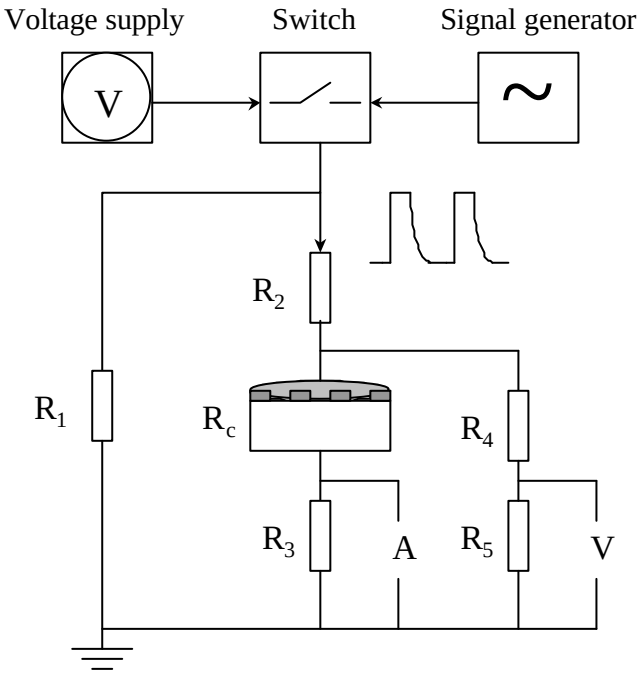

Fig. 5.3-1 Set-up for poling.

A DC voltage (<10 kV) is applied over the sample via a fast high voltage switch. The switch is operated with TTL pulses (5 V) from a signal generator. This generates high voltage pulses of arbitrary lengths, which are applied one by one by a manual trigger. Typical pulse lengths used in this work are 1-20 ms. The rise time of the pulses is short (<100 µs), while the fall time, which depends on R_1 and the sample size, is of the order of 1-2 ms. The longer fall time has been chosen to prevent back-flipping of domains after the voltage has been turned off. However, unlike in $LiNbO_3$, no tendencies of back-flipping have been observed in the KTP materials, which indicates a high degree of stability for the established domain walls.

The serial resistance R_2 provides a current control during poling (mainly for low-conductive samples), and can be adjusted to the conductivity of the sample (~100 kΩ-1 MΩ)[2]. The current through the sample is measured over a small serial resistance, R_3, while the voltage over the sample is measured by voltage division between R_4 and R_5 in a parallel circuit. R_4 is chosen large in order for the voltage measurements to be passive.

5.4 Preparation of the samples

The initial crystal wafers are z-cut with polished z-faces. Typical dimensions are 1-3 mm in thickness and 30x30 mm in the x-y plane (somewhat smaller for RTA). The wafers are first evaluated in terms of domain structure. This is accomplished by a piezo-electric mapping device. The results give an indication of the homogeneity of the crystal. In case there are multi domain structures the wafers have to be single-domain poled prior to patterning of periodic electrodes.

A set-up was also developed for mapping the conductivity over the wafer. Such measurements give valuable information on how samples cut-out from different parts of the wafer will behave during the poling process. The anode consists of an electrolyte that covers uniformly the c^+-face of the wafer while the cathode is a In-covered probe that can be connected at arbitrary positions over the c^--face. The contact area of the probe could be estimated by scanning the probe across an anode edge while measuring the current. This confirms the strong anisotropy of the conductivity. The measurements in fig. 5.4-1, made in KTP, indicate a probe diameter of 1 mm. All conductivity measurements are taken at 1.5 kV with 6 ms long pulses. The reason for the high voltage is to enable comparison of the conductivity over the wafer and between different wafers at close to poling conditions. The obtained current of 63 µA in fig. 5.4-1 yields an absolute value of the conductivity of $5.3*10^{-7}$ S/cm (6 ms pulses gives an equivalent frequency of ~170 Hz).

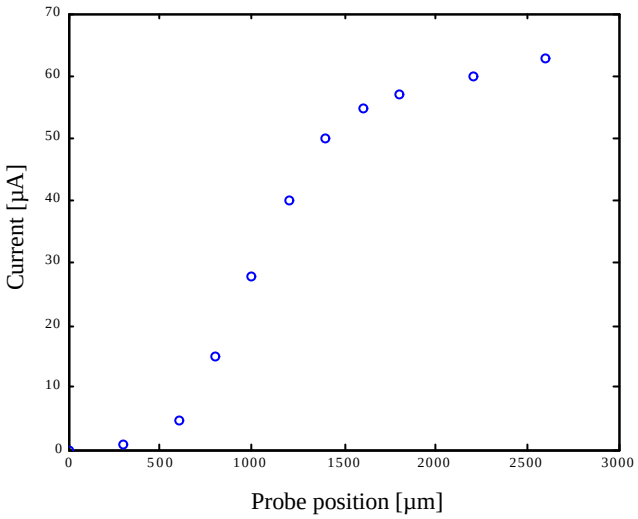

Fig. 5.4-1 Estimation of the conductivity probe area by scanning the probe across an electrode edge (KTP).

A typical map of the conductivity over a 15x15 mm wafer area is shown in fig. 5.4-2. As can be seen, the conductivity variation is almost parabolic along the y-axis with a 2-times difference between maximum and minimum. On the other hand, the conductivity remains fairly constant along the x-axis. This feature could perhaps be related to the temperature gradient during growth. The variation in conductivity is in general less pronounced in RTA and RTP.

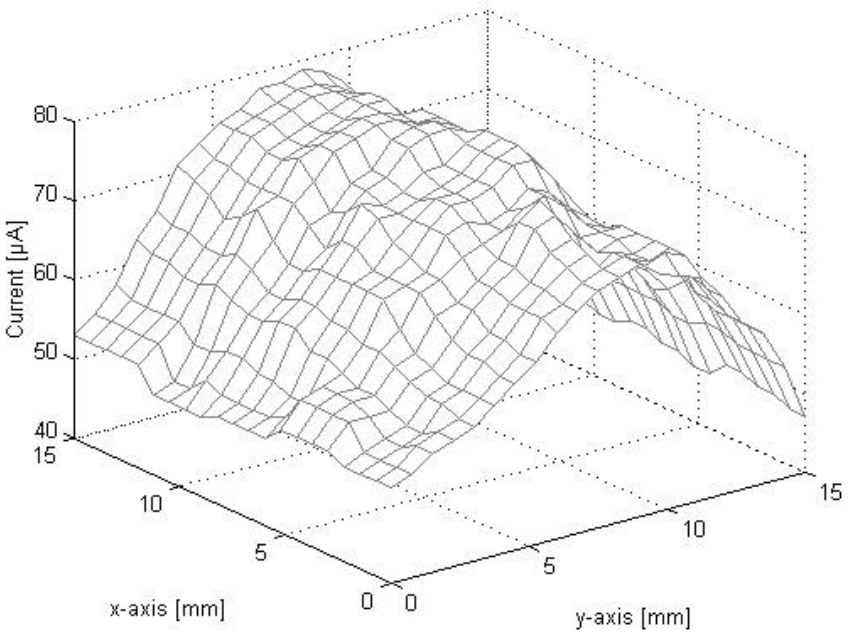

Fig. 5.4-2 Conductivity variation in flux grown KTP (China).

After evaluation, the wafers are cut into samples, the end-faces of which are polished for propagation along the x-axis. Typical sample dimensions are 5 mm wide (y-axis) and 5-20 mm long (x-axis).

The samples are then cleaned and patterned with periodic electrodes on one of the polar faces using standard lithographic methods. The photoresist layer has a thickness of 2 µm. Different types of electrode configurations were tested as illustrated in fig. 5.4-3.

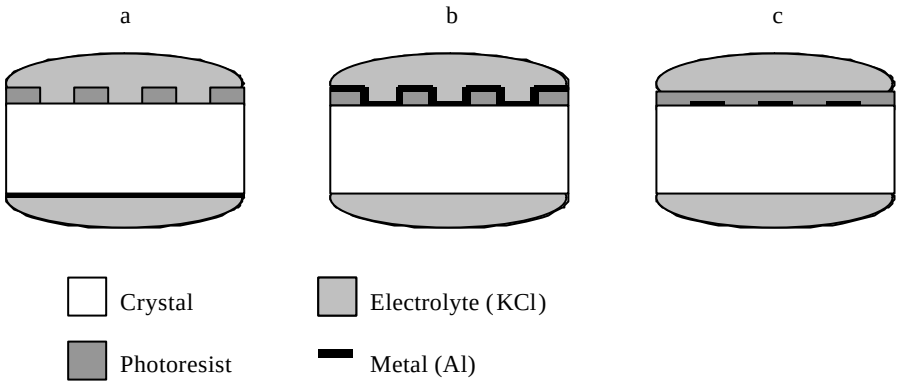

Fig. 5.4-3 Electrode configurations used for periodic poling.

The different configurations were also applied to the two polar faces of the crystals. Common for all configurations is that the photoresist is used as insulator. The electrolyte is a nearly saturated solution of KCl. Al was chosen as the metal since it is easily removed and since tests with other metals (Ti) did not show any noticeable differences in electric contact. It was difficult to unambiguously determine which electrode configuration is most suitable, since variations in material quality, even over the same crystal wafer, seem to have stronger influence on the poling results than the electrode configuration. Similarly was it difficult to distinguish any differences in terms of nucleation density and domain wall propagation features between placing the periodic electrode onto the c^+ or onto the c^- polar face.

However, some experiments indicate that the use of periodic metal electrodes, as compared to liquid electrodes, reduces the observed regions of nonlinearly “dead” material at the domain boundaries[A3]. This suggests that periodic metal electrodes might be most appropriate, especially for short period gratings. The main difference between (b) and (c) is that the insulating layer of photoresist in (c), can be made thicker, since it is spun-on after the photolithography. On the other hand, this configuration needs an additional processing step.

Furthermore, it was found experimentally that samples that had been poled once were easier to pole back to their original orientation. Pre-poling of the samples before patterning was therefore carried out in some experiments and seemed to have a positive effect on the quality of the domain structure, in particular for thick samples.

5.5 Monitoring the poling

In order to obtain a controlled poling process that can give reproducible results, it is of interest to be able to monitor the domain reversal in the crystal in some way. This is of special importance when working with materials from the KTP family, since their intrinsic irregularities prevent prediction of proper poling parameters.

Since high ionic conductivity makes it difficult to control the domain reversal by monitoring the poling current through the crystal, we have instead developed a method based on the transverse electro-optic effect in the crystal. In this way, we can monitor time-dependent changes in the polarisation-state of a He-Ne laser beam that propagates through the crystal during poling. The He-Ne beam is linearly polarised 45^{o} to the z- and y-axis of the crystal, and is launched along the x-axis of the crystal, see fig. 5.5-1.

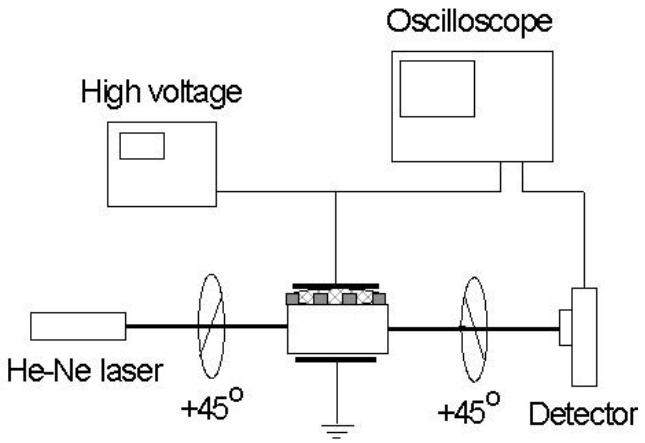

Fig. 5.5-1 Set-up for monitoring the poling process utilising the electro-optic effect.

When an electric field is applied to the crystal along the z-axis, the output polarisation-state of the He-Ne beam will be changed due to the electro-optic effect. This results in a time-dependent variation of the polarisation state during the rise and fall time of the electric pulse. During the rest of the pulse, when the voltage is constant, the polarisation-state will be time-dependent only if the sign of the electro-optic coefficients is reversed, i.e. if the crystal is being poled. The change in polarisation-state can be observed by measuring the intensity of the He-Ne beam through a polarisation analyser orthogonal to the initial polarisation.

The intensity at the detector during the rise and fall time of the voltage pulse without poling can be expressed as:

$$I \propto (1-\cos\Gamma) \qquad (5.5\text{-}1)$$

, where Γ is the time-dependent phase retardation between the y and z components of the beam:

$$\Gamma = \frac{2p}{l} E_z L \left(\frac{n_y^3}{2} r_{23} - \frac{n_z^3}{2} r_{33} \right) \qquad (5.5\text{-}2)$$

E_z is the applied electric field, n_y and n_z are the refractive indices for the two components, r_{23} and r_{33} the electro-optic coefficients, λ the wavelength of the He-Ne laser and L the length of the crystal.

With this method we have been able to observe how the poling proceeds through several distinct stages, characterised by different time constants. This confirms the theory for the domain reversal that was outlined in the beginning of this chapter. Since the electric field becomes homogenous in the crystal within a short distance from the patterned electrode, one can assume that a 50 % duty-cycle of poled and non-poled regions is obtained when the resulting electro-optic coefficient integrated over the whole crystal length is zero.

A typical oscilloscope trace of the poling of a 1 mm thick and 20 mm long periodically patterned KTP crystal is illustrated in fig. 5.5-2. The intensity modulation during rise time is not resolved in the image.

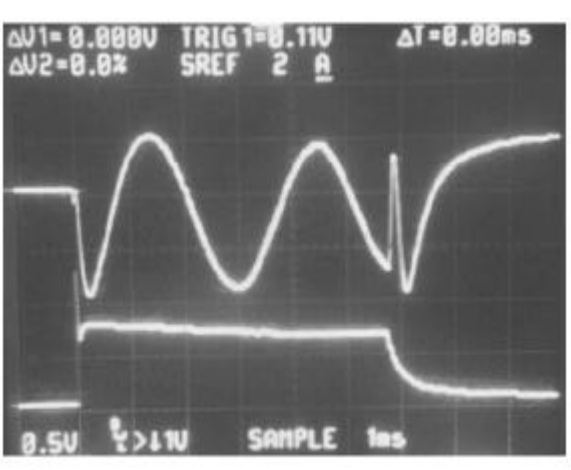

Fig. 5.5-2 Oscilloscope trace of optically monitored poling. The upper trace represents the intensity modulation while the lower is the voltage pulse.

The method has enabled controlled periodic poling of up to 3-mm thick samples of RTA and KTP and up to 1-mm thick samples of RTP[Paper III] (thicker RTP samples were never tested), and with periods as short as 2.95 μm (PPKTP)[Paper VIII].

5.6 Poling of flux grown KTP

Flux grown KTP is highly conductive compared to RTA and RTP, and therefore more difficult to pole periodically. Two possible ways of reducing the conductivity are doping the material with divalent or trivalent ions during growth[65-66], or reducing the temperature of the crystal to freeze the mobility of the ions. We have investigated Cr^{3+}-, Sc^{3+}- and Ga^{2+}-doped flux grown KTP and found that they exhibit up to two orders of magnitude lower conductivity. Unfortunately, the dopants seem to "lock" the lattice, which renders domain inversion impossible. On the other hand, Rosenman *et al.* have demonstrated successful periodic poling of KTP and KTA at low temperatures[67-69]. A drawback with poling at low temperatures is an increase in the coercive field[8].

In this work we have instead investigated a method based on ion-exchange to circumvent the problem of high conductivity. Immersing the KTP crystal in a bath of 100 % melted $RbNO_3$, results, through the exchange of K and Rb ions, in a low-conductive layer of $Rb_xK_{1-x}TiOPO_4$ (Rb:KTP) at the two c-faces (x varies gradually from 100 % at the surface to 0 in the bulk)[70-71]. During poling of such crystals the domains will first nucleate in the exchanged layers, where the field is much larger than in the bulk due to voltage division between the low-conductive surface layer and the high-conductive bulk. The lower field in the bulk is however still sufficient to drive the established domains along the z-direction towards the opposite side. We have found that fields of less than 1 kV/mm are enough to drive domains through the bulk. By applying a uniform metal film on one side before the exchange process, one can force the nucleation to start exclusively at one side of the crystal and thereby limit the domain propagation to one single direction.

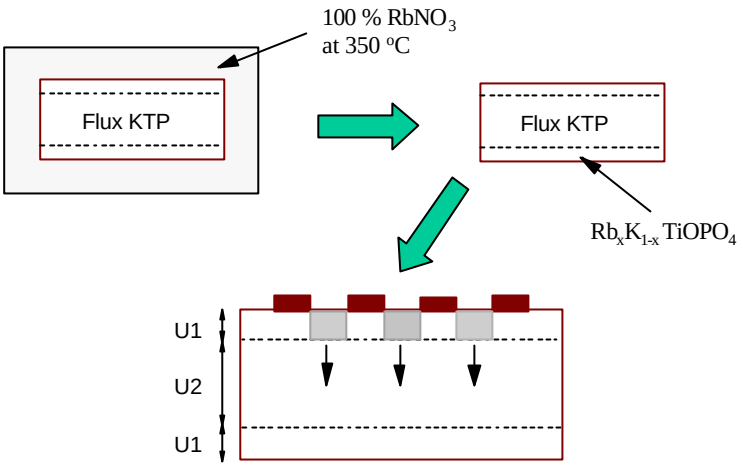

Fig. 5.6-1 Ion-exchange process for poling of flux grown KTP.

The induced Rb depth profile has been found to fit the complementary error function[5]:

$$C = erfc\left(\frac{z}{2\sqrt{Dt}}\right) \qquad (5.6\text{-}1)$$

C is the Rb concentration, z the depth in the crystal and t the time. The diffusion constant depends strongly on the exchange temperature and the vacancy concentration in the actual material. At temperatures around 350 °C we obtained Rb-layer depths (1/e) of 2-5 µm in the KTP material for exchange times of 3-8 hours. The depths were estimated from frequency dependent impedance measurements[72]. Such exchanged crystals of 1 mm in thickness exhibited a reduction of the total conductivity of up to 50 %, which indicates that there is a more than two orders of magnitude large difference in conductivity between the exchanged layer and the bulk. As opposed to ion-exchange with Rb^+/Ba^{2+}, we never observed any domain reversal on neither c^+ nor c^- caused by the ion-exchange itself. Ion-exchange with 100% Rb^+ is also much slower than for melts with even very small amounts of Ba^{2+} incorporated.

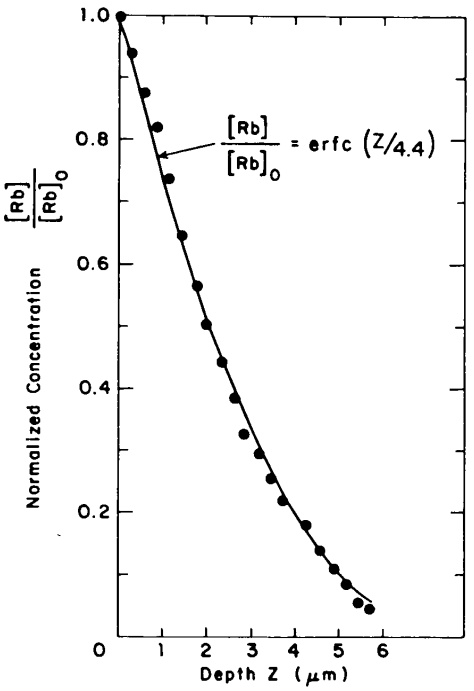

Fig. 5.6-2 Exemple of induced Rb depth profile measured using an electron microprobe[5].

Interestingly, the ion-exchange also seems to have an equalising effect on the conductivity properties over the crystal wafer. If for simplicity it is assumed that the diffusion scales linearly with the original crystal conductivity at a certain point on the wafer, it turns out that the variation in total conductivity (bulk plus ion-exchanged layers) over the wafer after the exchange process is considerably reduced. This is illustrated in fig. 5.6-2. Moreover, it appears that for variations in conductivity similar to what we have measured in virgin wafers, a maximum decrease in variation is obtained when the absolute conductivity (at maximum) is reduced with about 30-40 %. This effect might have an advantageous influence on the quality of the domain structures, by contributing to making the poling more homogenous.

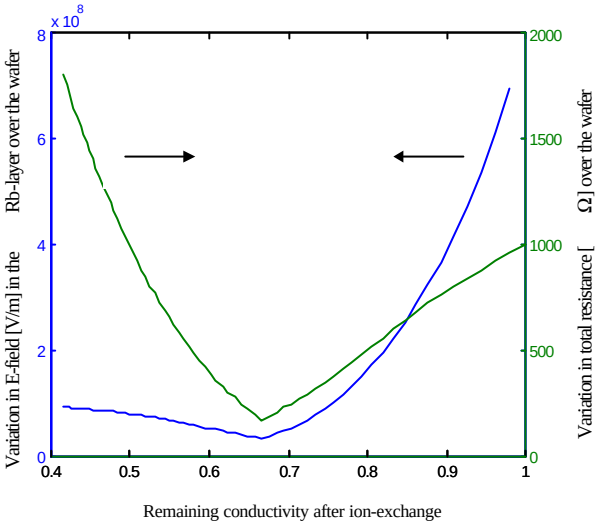

Fig. 5.6-2 Variation (max - min) in E-field (in Rb-layer) and in total conductivity versus ion-exchange time in terms of remaining total conductivity (max conductivity before exchange divided by max conductivity after exchange) over a KTP wafer which originally had a conductivity variation of $5*10^{-7}$-$1*10^{-6}$ S/cm.

The ion-exchange method described here was applied to all poling of flux grown KTP in this work and enabled fabrication of up to 3-mm thick PPKTP crystals (thicker crystals were never investigated).

5.7 Evaluation of domains

It has been found that the domain structures in the crystals can be revealed after poling by selective etching techniques[73]. This can give valuable information about the quality of the introduced QPM structure. In this work, we have used a 2:1 mole ratio water solution of KOH and KNO_3[74] at about 80 ^oC, which selectively attacks the c^--face of the crystal. The same solution has been used for KTP as well as RTA and etching times varies between 5-20 min[PaperVIII].

Fig. 5.7-1 is a microphotograph of a 1 mm thick periodically poled KTP sample with a period of 5.53 µm (for first-order SHG into the blue). Fig. 5.7-1(a) shows the c^--face, which was patterned with a periodic electrode, while fig. 5.7-1(b) is the uniformly patterned c^+-face. As can be seen, the domain structure is of good quality with close to 50 % duty-cycle on the c^-face, and most of the domains have propagated without significant broadening to the c^+-face.

From such etching evaluation, we have noted that domain broadening is strongly limited in the KTP materials. On the other hand, there is often a problem with missing domains over certain areas in the x-y plane. This can, among other things, probably be attributed to crystal inhomogeneities, which cause the poling conditions to be non-uniform over the sample.

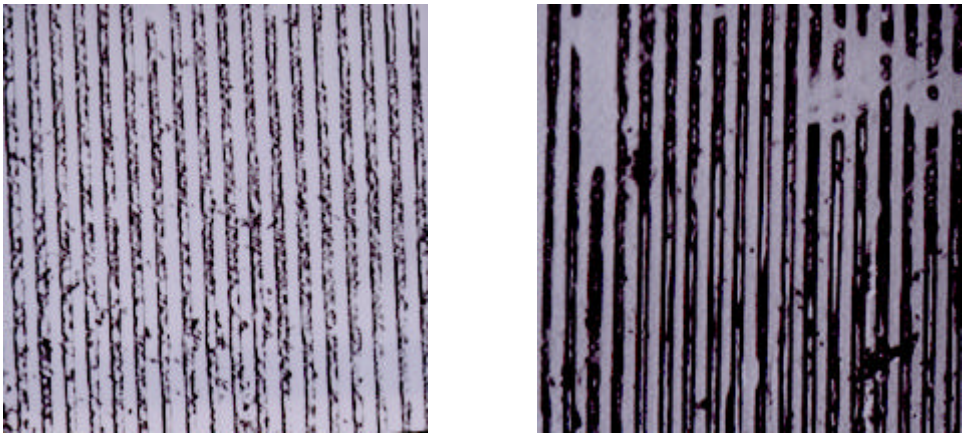

(a) (b)

Fig. 5.7-1 Domain structures in KTP revealed by selective etching on (a) c^--face (periodically patterned) and on (b) c^+-face (uniformly patterned).

6 Optical applications of PPKTP materials

6.1 Continuos wave SHG

SHG is the most straightforward type of optical experiment with QPM crystals. The fundamental beam from the pump source is focused into the QPM crystal, which is preferably mounted on a translation stage with a thermo-electric control. For type-I QPM processes, the pump beam should be linearly polarised along the crystal z-direction. The SH signal can be separated from the pump by a filter before being detected with a power meter.

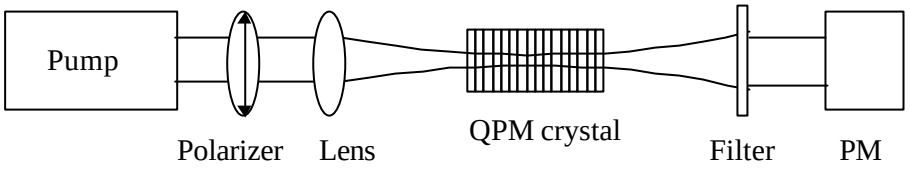

Fig. 6.1-1 Set-up for single-pass SHG.

The quality of the pump beam and the focusing conditions are critical for the conversion efficiency. Optimal focusing of gaussian beams is obtained (to a good approximation) when the beam diameter at the entrance and exit of the crystal is $\sqrt{2}$ times the beam waist inside the crystal[75,10]. This is confocal focusing. Through gaussian optics, confocal focusing imposes that the beam waist inside the crystal should be:

$$w_0^2 = \frac{lL}{2pn} \qquad (6.1\text{-}1)$$

, where λ is the pump wavelength, L is the crystal length and n the refractive index of the crystal at given pump wavelength. Inserting pw_0^2 as the overlap area into eq. 2.1-10 and adding a factor of 2 for taking into account a multimode pump[76] results in the following expression for the optimum conversion efficiency for QPM SHG of non-depleted gaussian beams:

$$h_{nd} = \frac{P_{SH}}{P_F} = \frac{128 d_{33}^2 P_F L}{m^2 n_F n_{SH} l_F^3 e_0 c} \sin c^2\left(\frac{\Delta kL}{2}\right) \qquad (6.1\text{-}2)$$

The effective nonlinear coefficient, d_{eff}, has here been replaced with the characteristic nonlinearity for type-I QPM interactions, $d_{eff} = \frac{2}{mp} d_{33}$, where m is the order of QPM. A calculation shows that normalised conversion efficiencies of about 1%/Wcm should be possible to attain with QPM crystals of perfect quality from KTP materials (for generation in the visible/UV).

For improved optical-to-optical efficiency it is of interest to make cw SHG in an intra-cavity configuration, which has the advantage of utilising the high intensity of the circulating pump field. In this way, we have been able to obtain over 700 mW of cw blue light by SHG in PPKTP with a total optical-to-optical efficiency exceeding 5%[PaperVI]. An alternative way of attaining higher conversion efficiencies is to place the nonlinear crystal in an external cavity[77].

The effective length of the QPM grating in the crystals can be estimated by measuring the width of the phasematching peak. The phasematching characteristics can conveniently be reproduced experimentally by tuning the pump wavelength or the crystal temperature, yielding the acceptance bandwidths $\Delta\lambda$ or ΔT. The grating length can then be derived using[14]:

$$\Delta l = \frac{0.4429\, l_F}{L}\left[\frac{n_{SH} - n_F}{l_F} + \frac{\partial n_F}{\partial l_F} - \frac{1}{2}\frac{\partial n_{SH}}{\partial l_{SH}}\right]^{-1} \qquad (6.1\text{-}3)$$

$$\Delta T = \frac{0.4429\, l_F}{L}\left[\frac{\partial n_{SH}}{\partial T} - \frac{\partial n_F}{\partial T} + \alpha\left(n_{SH} - n_F\right)\right]^{-1} \qquad (6.1\text{-}4)$$

In eq. 6.1-4, α is the thermal expansion coefficient of the material. It should be pointed out that loose focusing conditions are needed in order to obtain non-distorted phasematching characteristics.

The simplicity of single-pass SHG makes this experiment a useful tool for evaluating the quality of the fabricated QPM structures, especially if the pump source is a tuneable laser. With a Ti:Sapphire laser (continuously tuneable from ~750-1000 nm) it is possible to characterise not only QPM crystals meant for SHG to the visible, but also crystals for other applications (with longer grating periods) by detecting the SH signals from higher-order QPM. An example of this is shown in fig. 6.1-2. Three phasematching peaks corresponding to 7:th, 8:th and 9:th order QPM SHG were obtained from a PPKTP sample with a period of 31 μm by scanning the Ti:Sapphire laser over 810-870 nm[PaperII]. The corresponding first-order periods are 31/7=4.42 μm

(7:th-order), 31/8=3.87 µm (8:th-order) and 31/9=3.44 µm. A close-up of the 7:th-order peak shows that it resembles the typical sinc^2-like phasematching characteristics.

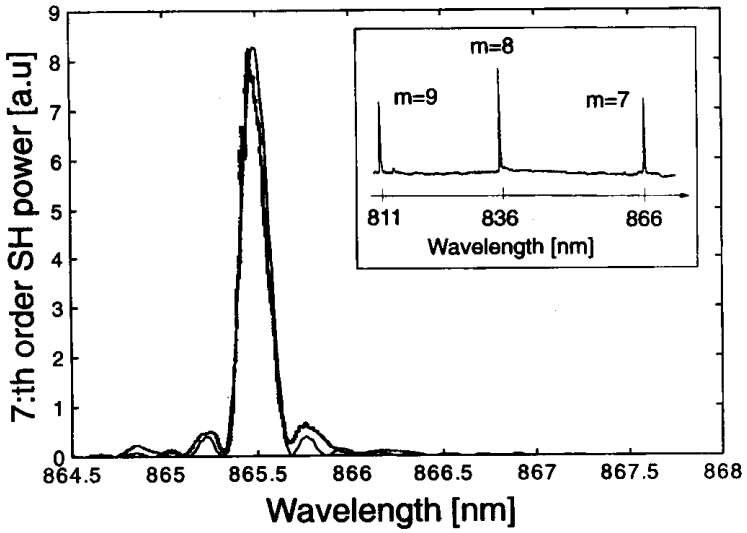

Fig. 6.1-2 Higher-order QPM SHG in PPKTP with a period of 31 µm.

However, it should be noted that the SH power generated in a laminar QPM structure (at phasematching) is determined by[78]:

$$P_{SH} \propto \frac{4}{p^2 m^2} \sin^2\left[m \frac{2p}{\Lambda}\left(\frac{\Lambda}{4} + \frac{d}{2}\right)\right] P_F^2 \qquad (6.1\text{-}5)$$

, where Λ is the QPM period and δ is the discrepancy in l (see section 3.1) from $\Lambda/2$ (the expression is derived by calculating the Fourier coefficient for a laminar structure). From this it follows that the conversion efficiency for higher-order QPM is very sensitive to small deviations in duty-cycle. A calculation shows, for example, that a deviation of less than 5 % in δ allows the 8:th-order peak to appear with a peak power of the same magnitude as the 7:th-order peak (all even-order peaks are 0 for δ=50 %).

By translating the QPM crystal transversally (in the y-z plane) with respect to the pump beam while detecting the SH power, one can obtain important information about the homogeneity of the QPM structures over the available aperture (if the pump diameter is considerably smaller than the crystal aperture). Fig. 6.1-3 shows a 2-dimensional plot of the 6:th-order SH output from a 3 mm thick and 9 mm long PPKTP crystal with a period of 37.8 µm. The pump wavelength was 955 nm and the pump diameter was ~50 µm. The small variation in the signal indicates a good homogeneity of the QPM grating over the whole aperture. The sample was later used in a nano-second OPO pumped with a large 1064 nm beam (~2 mm in diameter), which generated up to 11 mJ pulses

at a signal wavelength of 1.72 µm (the signal output energy was limited by available pump energy, 28 mJ).

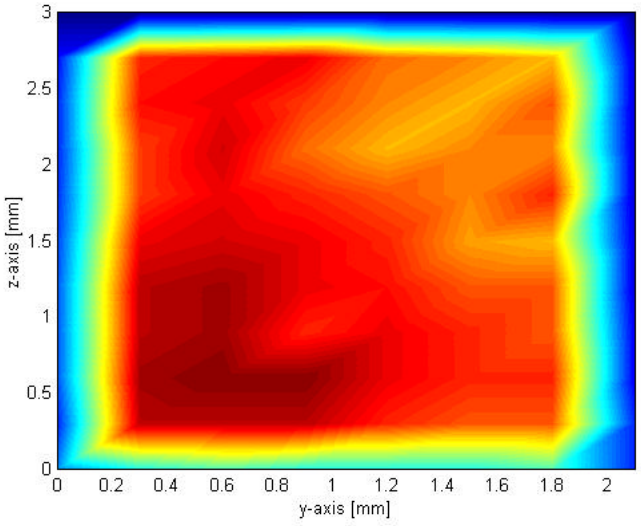

Fig. 6.1-3 6:th-order SH power across the aperture of a 3 mm thick PPKTP crystal.

6.2 Pulsed SHG

SHG of pulsed lasers gives significantly larger conversion efficiencies, due to higher fundamental peak intensities. In paper V we demonstrated for instance conversion efficiencies exceeding 65 % for SHG into the green from nano-second pulses at 1064 nm from a Nd:YAG laser. In this case, it is necessary to take pump depletion into account in the calculations of the conversion efficiency, yielding (for Δk=0)[10]:

$$h_d = \frac{\overline{P}_{SH}}{\overline{P}_F} = \tanh^2\left[(h'_{nd})^{1/2}\right] \qquad (6.2\text{-}1)$$

, where $\overline{P}_{SH}$ and $\overline{P}_F$ are the second-harmonic and fundamental average power respectively. For pulses with Gaussian temporal shape the relation between h'_{nd} and h_{nd} is the following[79]:

$$h'_{nd} = h_{nd}\left[\left(\frac{2\ln 2}{p}\right)^{1/2}\right]\frac{1}{tf} \qquad (6.2\text{-}2)$$

, where τ is the full width half maximum (FWHM) pulse duration and f is the pulse repetition rate.

Pump depletion saturates the increase in conversion efficiency at high power levels. In practical applications, especially for SHG into the visible, the conversion efficiency is also limited by the enhanced residual absorption of the second-harmonic wave inside the nonlinear crystal. This implies that the length of the crystal has to be optimised for maximum output (i.e. a shorter crystal can give better conversion efficiency than a longer one).

For ultra-short pulses, i.e. shorter than picoseconds, the group-velocity dispersion in the crystal starts to play an important role in the nonlinear process. Temporal walk-off between the fundamental and the second-harmonic wave induces a group velocity mismatch, Δu^{-1}, which limits the effective interaction length, L_w in the crystal[80]:

$$L_w = \left(\left| \Delta u^{-1} \right| \Delta w_F \right)^{-1} \tag{6.2-3}$$

, where $\Delta\omega_F$ is the spectral width of the fundamental pulse (for transform-limited fundamental pulses with a duration of τ_F, one has: $\tau_F \Delta\omega_F \sim 1$). The group-velocity mismatch can be expressed as[80]:

$$\Delta u^{-1} = \frac{1}{c}\left(n_{SH} - n_F - l_{SH} \frac{\partial n_{SH}}{\partial l_{SH}} - l_F \frac{\partial n_F}{\partial l_F} \right) \tag{6.2-4}$$

Furthermore, the group-velocity dispersion causes temporal broadening of the fundamental and second-harmonic pulses.

6.3 Optical Parametric Oscillators (OPO's)

The down conversion processes described in section 2.1 are normally very weak compared to SHG, SFG and DFG, since there are no input photons at the signal or idler. However, by resonating one or several of the interacting beams, an Optical Parametric Oscillator is obtained, an efficient device somewhat similar to a laser with a gain medium, resonator conditions and oscillation threshold[11,81]. Depending on the number of resonated waves, the devices are named single-resonant OPO (SRO), double-resonant OPO (DRO)[82] or triple-resonant OPO (TRO)[83].

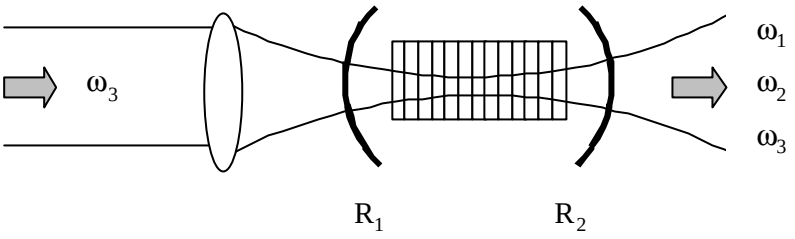

Fig. 6.3-1 Schematic illustration of a linear cavity OPO.

The signal and idler beams start up from noise and are amplified during the round-trips in the cavity. Threshold is reached when the gain equals the cavity losses. Considerably lower thresholds can be achieved in DRO's and TRO's, but those suffer from high sensitivity to perturbations and limited continuos wavelength tuning for single-longitudinal mode devices, which make necessary the use of dual cavities. Therefore, SRO's are most useful in practical applications. The total optical-to-optical conversion efficiency can be considerably increased for SRO's by employing intra-cavity configurations[84].

Normalising the fields in eq. 2.1-6 in terms of photon flux ($A_m(x) = \left(\frac{n_m}{w_m}\right)^{\frac{1}{2}} E_m(x)$) and assuming no pump depletion ($A_3(x) = A_3(0)$) yield[10]:

$$\begin{aligned}
\frac{dA_1}{dx} &= -\frac{g_1}{2}A_1 - i\frac{g}{2}A_2^* \\
\frac{dA_2}{dx} &= -\frac{g_2}{2}A_2 - i\frac{g^*}{2}A_1 \\
g &= \frac{d_{eff}}{c}\sqrt{\frac{w_1 w_2 w_3}{n_1 n_2 n_3}}A_3(0)
\end{aligned} \qquad (6.3\text{-}1)$$

$\gamma_{1,2}$ represent here the total round-trip losses in the cavity. By applying the Manley-Rowe relations, i.e.:

$$\frac{d}{dx}|A_1|^2 = \frac{d}{dx}|A_2|^2 = -\frac{d}{dx}|A_3|^2 \qquad (6.3\text{-}2)$$

the following solutions are obtained for the signal and idler photon fluxes:

$$\begin{aligned}
A_1(x) &= A_1(0)ch\frac{G}{2}x - i\frac{g}{G}A_2(0)^* sh\frac{G}{2}x \\
A_2(x)^* &= A_2(0)^* ch\frac{G}{2}x + i\frac{g}{G}A_1(0)^* sh\frac{G}{2}x
\end{aligned} \qquad (6.3\text{-}3)$$

, where $G^2 = gg^*$. Oscillation threshold is reached when the gain equals the round-trip losses in the cavity. The pump intensity thresholds for DRO's and SRO's become:

$$\text{DRO: } g_1 g_2 = G^2 \Rightarrow I_3^{th} = \frac{\varepsilon_0 c^3 n_1 n_2 n_3}{2\omega_1 \omega_2} \frac{\Gamma_1 \Gamma_2}{d_{eff}^2 L^2} \qquad \text{(6.3-4 a)}$$

$$\text{SRO: } A_1(L) = A_1(0) \Rightarrow I_3^{th} = \frac{\varepsilon_0 c^3 n_1 n_2 n_3}{\omega_1 \omega_2} \frac{2\Gamma_1}{d_{eff}^2 L^2} \qquad \text{(6.3-4 b)}$$

L is here the crystal length and Γ_m are the round-trip losses expressed as $\Gamma_m = -\ln\left[R_{1m} R_{2m} (1-\beta_m)\right]$, where $R_{1,2m}$ are the reflection coefficients of the cavity mirrors at each wavelength. β_m comprises all other losses inside the cavity (assuming no absorption).

An analytic expression for the SRO threshold of a pulsed OPO with a Gaussian temporal profile was derived by Brosnan and Byers (assuming no walk-off)[11]:

$$I_3^{th} = \frac{2.25}{k g_s L^2} \left[\frac{L_c}{2tc} \ln(33) + 2\alpha_{1,2} L + \ln \frac{1}{\sqrt{R_{1,2}}} + \ln 2 \right]^2 \qquad \text{(6.3-5)}$$

, with $k = \frac{2\omega_1 \omega_2 d_{eff}^2}{n_1 n_2 n_3 \varepsilon_0 c^3}$ and $g_s = \frac{r_3^2}{r_3^2 + r_{1,2}^2}$, where ρ_m are the Gaussian mode radii of the beams. L_c is the optical cavity length and τ is the pulse length.

The significant advantage of using QPM in OPO's depends on the type of OPO. For cw OPO's, where mode-matching and high gain is of critical importance, both the non-critical phasematching schemes and the high nonlinearity provided by QPM are advantageous. In pulsed OPO's, where the gain is much higher due to increased peak intensities, the high nonlinearity is not so critical. Nevertheless, femto-second[85,A1], pico-second[79,PaperVIII], and high repetition-rate nano-second OPO's[86], which are most often mode-matched, benefit strongly from non-critical phasematching. QPM therefore contributes to increasing the flexibility of such OPO's systems in terms of operation wavelengths and tunability. Moreover, it has been proven that the use of one single polarisation in combination with high nonlinearity in QPM OPO's enable generation of wavelengths further out in the IR than in the case of conventional OPO's[56,57]. In the case of low-repetition rate nano-second OPO's[87], which do not normally require neither high gain nor mode-matched cavities, it is of more importance that the nonlinear crystal provides good energy handling capability and large apertures.

A variety of OPO's, based on PPRTA and PPKTP, have been realised in this work, including both pulsed OPO's (nano-second - high/low-rep.rate[PaperIV], pico-second[PaperVIII] and femto-second[A1]) and cw OPO's[A2]. Significant for these OPO's was the capability of performing stable operation at room temperature, even at high power or energy levels. However, it was observed from OPO experiments that most of the available Sellmeier equations are not accurate enough above 1 µm to allow correct prediction of the QPM period in the IR, see fig. 6.3-1.

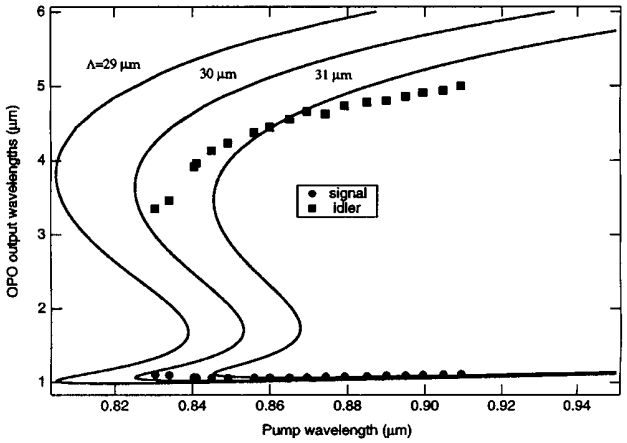

(a)

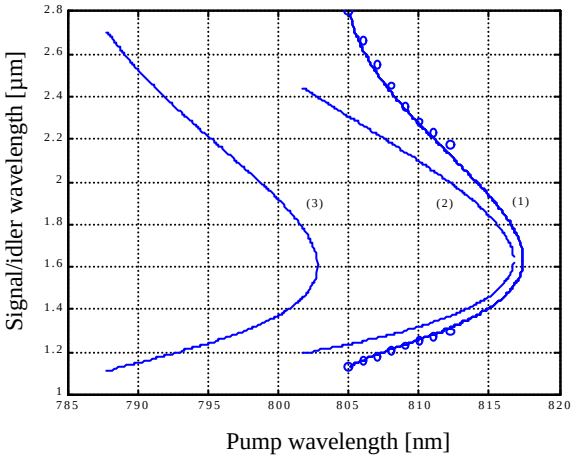

(b)

Fig. 6.3-1 Examples of OPO's based on (a) PPRTA[PaperVII] (ps OPO, l=30 µm) and (b) PPKTP (cw OPO, l=27.5 µm) illustrating the discrepancies between experimentally obtained wavelengths and predictions from Sellmeier data. The Sellmeier data used in (a) is from Fenimore[50], and the curves in (b) correspond to (1) Fradkin[52], (2) Dyakov[48] and (3) Kato[49].

6.4 Type-II QPM

During SHG experiments using a Ti:Sapphire laser as a pump, it was discovered that for a certain QPM period it was possible to obtain an additional phasematching peak at a different wavelength by turning the linear pump polarisation with respect to the crystal axes. The measurements indicated that the additional phasematching peak corresponded to a type-II QPM process in which the z- and y-components of the pump beam are coupled via the d_{24} tensor element (the possibility to obtain type II QPM was not known to the author before this, but it turned out later that the phenomenon had been discussed earlier[88]). The phasematched wavelength is then given by:

$$\Lambda = \frac{m l_F}{2n_{SH}^y - n_F^z - n_F^y} \qquad (6.4\text{-}1)$$

Obviously, periodic reversal of the spontaneous polarisation along the z-axis had given rise to a spatial modulation not only of the d_{33} coefficient but also of the d_{24} coefficient. The reason for this is not clear. Crystallographically, it is reasonable to believe that the crystal axis symmetry remains constant during poling, i.e. reversal of the z-axis imposes reversal of either the y- or the x-axis. A number of crystals were examined, and they all exhibited type-II phasematching characteristics, indicating that the y-axis is always reversed along with the z-axis. However, further investigations of these observations are motivated.

Nevertheless, type-II QPM processes can be interesting for several reasons. First, short wavelength generation can be achieved using much longer QPM periods than in the case of type-I processes, since the crystal's birefringence is utilised, see fig. 6.4-1[PaperIX]. This relieves somewhat the constraints on the fabrication process for short period structures. Second, the wavelength acceptance is wider in type-II processes, which might be an advantage in short pulse SHG. Finally, in some OPO applications it might be useful to obtain the output signal and idler beams in orthogonal polarisation directions. However, it should not be forgotten that the d_{24} coefficient is significantly smaller than the d_{33} coefficient, which reduces the conversion efficiency of the process.

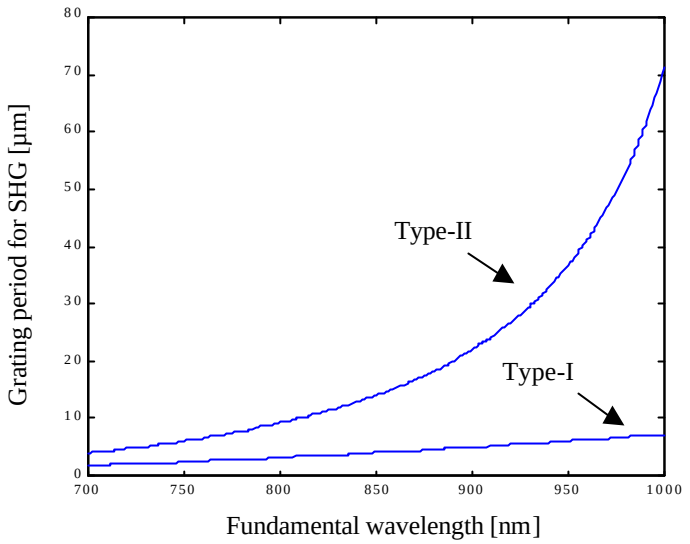

Fig. 6.4-1 Comparison of required QPM period for SHG between type-I and type-II processes in PPKTP.

6.5 Damage

Optically induced damage in the crystals puts fundamental limitations on their performance in practical applications. Damage thresholds depend strongly on several parameters such as average intensity, pulse peak intensity, pulse energy, pulse length, wavelength and absorption. This makes studies of optical damage fairly complicated, and it is more or less impossible to determine any general values of a material's damage thresholds. A number of different distinct types of damage have been identified:

1. *Photorefractive damage*[89]*:* This effect is caused by optically excited free charges in the crystal, which diffuse in the electro-magnetic field of the light beam. They get trapped outside the beam and set up an internal field, which distorts the beam via the electro-optic effect. Photorefractive damage can often be annealed at elevated temperatures[15]. It has also been shown that a QPM structure in the crystal considerably reduces the effects of photorefractive damage due to charge neutralisation between adjacent domains and decreased average electro-optic beam deflection[90]. Nevertheless, photorefractive damage is indeed a limiting factor when trying to use PPLN for high power and short wavelength generation applications. The KTP materials, on the other hand, are known to have several orders of magnitude higher resistance to photorefractive damage than $LiNbO_3$. A suggested reason for this is their higher conductivity.

2. *Gray-tracks:* It has been observed that high intensities, especially at short wavelengths, may give rise to formation of gray tracks along the light beam[91-93]. Those tracks are due to a dramatic increase of the absorption in the visible, which has been attributed to the presence of excited colour centres in the crystal in the form of Ti^{4+}. The formation of gray-tracks depends both on the intensity and the wavelength of the exposing beam. It has also been argued that there are different mechanisms involved with different time constants[94]. Large differences in sensitivity to gray-track formation have been observed between different material qualities, and are probably related to differences in impurity level and conductivity. For instance, hydrothermal KTP and high-conductive flux grown KTP seem to be much more resistant to gray-track formation than other KTP qualities. Gray-tracks can, like photorefractive effects, to some extent be avoided by thermal annealing.

3. *Material breakdown:* At some intensity levels, the optically induced strain leads to permanent collapse of the material[11]. Such damage is probably initiated by temperature increases due to absorption. Damage can occur both at the crystal surfaces due to surface effects and crystal structure defects close to the surface induced by the polishing, or in the bulk due to crystal imperfections and self-focusing. The higher residual absorption and the possible creation of colour centres due to multi-photon absorption for shorter wavelengths make the damage thresholds considerably lower for visible light. In experiments with green light generation by SHG of 1064 nm, we have observed higher damage threshold for PPKTP than for bulk KTP. The reason for this might be that the residual absorption is lower for the use of one single polarisation, or that the materials originated from different suppliers.

Table 6.5-1 below is meant to give a summary of the collected experience regarding damage thresholds, or rather absence of damage, in PPKTP and PPRTA taken from various optical experiments. The values given are the maximum intensity levels that have been launched into or generated inside the crystals, limited either by available power or by damage:

Material	**Wavelength [nm]**	**Pulse time**	**Average intensity [kW/cm^2]**	**Peak intensity [MW/cm^2]**	**Type of Damage**
PPKTP	1064+ 532	220 ns	18.7+ 23.4	71+ 89	Break-down
PPKTP	1064+ 532	cw	305 10.0	-	None
PPKTP	1053+ 526.5	150 ns	36.7+ 29.8	24.5 19.9	Breakdown
PPKTP	946+ 473	cw	157+ 2.0	-	None
PPKTP	780+ 390	100 fs	15.2+ 0.2	3000+ 126	None
PPKTP	1064+ 1800	5 ns	0.090+ 0.020	900+ 205	None
PPRTA	1064+ 1580	20 ns	-	103+ 27	None
PPRTA	850+ 1070	1.5 ps	198+ 38.5	1630+ 317	None

Table 6.5-1 Maximum intensity levels used in optical experiments with PPKTP and PPRTA.

7 Description of included papers

Paper I: Frequency doubling in periodically poled $RbTiOAsO_4$

Periodic poling of RTA is demonstrated for the first time. A 3-mm long and 1-mm thick sample was patterned with a 4.2-µm photoresist grating using standard photolithography and poled at 2.5 kV/mm. The sample was used to obtain first-order SHG from a Ti:Sapphire laser tuned at 873 nm. An output power of 270 µW at 436.5 nm was obtained for an IR input of 490 mW, yielding a conversion efficiency of 5.5 x 10^{-4}. The influence of missing domains in the QPM structure on the phasematching characteristics was studied.

Paper II: Electric field poling of flux grown $KTiOPO_4$

A method for poling of flux grown KTP with high ionic conductivity is developed. Ion-exchange with Rb ions creates low-conductive layers at the surfaces, were nucleation is initiated when a high voltage is applied. Samples were poled at about 2 kV/mm and effective d_{33} coefficients as high as 16.9 pm/V were presented. First-order frequency doubling of a Nd:YAG was achieved in a 1-mm thick PPKTP sample at room temperature with a period of 9.01. Higher-order SHG was obtained from a 31-µm structure using a tuneable Ti:Sapphire. The sensitivity of the conversion efficiency to variations in duty-cycle for higher-order QPM was discussed.

Paper III: Periodic poling of $RbTiOPO_4$ for quasi-phase matched blue light generation

RTP is introduced for the first time as an interesting candidate for periodic poling due to its low conductivity. A novel method for monitoring the poling process based on the electro-optic effect is described. This method enabled fabrication of QPM structures with good homogeneity through the whole sample thickness. Poling of 1-mm thick samples occurred at 3.9 kV/mm. Blue light generation was obtained by frequency doubling Ti:Sapphire laser radiation at 984 nm inside a PPRTP sample with a period of 6.63 µm. SHG experiments were also carried out with a InGaAs diode laser.

Paper IV: Nanosecond optical parametric oscillator based on large-aperture periodically poled $RbTiOAsO_4$

A 3-mm thick sample of RTA, patterned with a period of 40.2 µm was poled at 5.3 kV/mm. This is the thickest periodically poled crystal that has ever been demonstrated.

The PPRTA crystal was evaluated in two different ns-OPO's pumped by Nd:YAG lasers. The first was a high repetition rate (1kHz, 5 ns) OPO with very good beam quality, which was used to study the nonlinearity and homogeneity of the PPRTA crystal. The results indicated an effective d_{33} coefficient well above 10 pm/V over the whole aperture (3x3 mm). This large aperture was utilised in the second OPO (10 Hz, 20 ns) to produce up to 17 mJ of signal pulse energy at 1.58 μm.

Paper V: Efficient Nd:YAG laser frequency doubling with periodically poled KTP

Detailed measurements on green light generation in 1-mm thick PPKTP were carried out. Continuous wave as well as pulsed frequency doubling was investigated. A maximum conversion efficiency of 66% was obtained for ns pulses. Saturation effects due to absorption and thermal heating were studied. The reproducibility of the poling process was estimated by comparing several equally processed samples. The QPM crystals were also compared with conventional type-II frequency doublers, and were found to be about two times more efficient.

Paper VI: Generation of 740 mW of blue light by intra-cavity frequency doubling with a first-order quasi-phase-matched $KTiOPO_4$ crystal.

The high power of the circulating field at 946 nm inside a diode-pumped quasi-three level Nd:YAG laser was used to produce up to 740 mW of cw blue light from a PPKTP crystal. The PPKTP crystal was 1 mm thick and 9 mm long and had a grating period of 6.09 μm. The blue output was stable up to 500 mW. Above this level thermal lensing and possibly photorefractive effects caused fluctuations in the laser behaviour. Slight cooling of the crystal was needed to compensate for the absorption-induced heating at the highest pump levels. Neither gray-tracks nor permanent damage of the crystal occurred during the experiments.

Paper VII: Ultraviolet generation by first-order frequency doubling in periodically poled $KTiOPO_4$

A domain-inverted period of as short as 2.95 μm in a 9-mm long and 1-mm thick KTP crystal was used for first-order QPM SHG into the UV at 390 nm. A normalised conversion efficiency of 1.1%/Wcm was achieved in cw mode. The influence of group-velocity walk-off and pump bandwidth on the conversion efficiency for SHG of ultra-short pulses was studied.

Paper VIII: Near-to mid-infrared picosecond optical parametric oscillator based on periodically poled $RbTiOAsO_4$

A 5-mm long sample of PPRTA with a period of 30 μm was used as nonlinear medium in a synchronously pumped ps-OPO. The pump source was a self-mode-locked Ti:Sapphire laser, and pump tuning enabled continuous tuning of the output in the range of 3.35-5 μm. Total output average powers of 400 mW in ~1 ps pulses were obtained at 33% extraction efficiency. The OPO was operated at room temperature and no sign of photorefractive damage was observed in the PPRTA crystal.

Paper IX: First-order type II quasi-phase-matched UV generation in periodically poled KTP

A type II quasi-phasematched configuration was studied for the first time. Radiation at 398.8 nm was obtained by frequency doubling a Ti:Sapphire laser in a 8.5-mm long and 1-mm thick PPKTP crystal with a period of 9.01 μm. The utilised effective d_{24} coefficient was measured to 2.82 pm/V. Phasematching characteristics were studied in terms of wavelength tuning as well as temperature tuning.

8 Conclusions

A process for fabrication of QPM structures in bulk crystals from the KTP family by periodic electric field poling has been developed. The materials that have been studied are KTP, RTA and RTP. High ionic conductivity and limited homogeneity of virgin crystals have been identified as the main problems with these materials. The former has been circumvented by using the less conductive materials RTA and RTP and by employing an ion-exchange technique for KTP. For the latter we have developed a new method to monitor the domain reversal based on the electro-optic effect.

The process developed has enabled fabrication of QPM structures of good quality in up to 3-mm thick samples of RTA and KTP and in up to 1-mm thick samples of RTP. Those PP-crystals have been used in a large variety of optical experiments including both SHG into the visible/UV and OPO's operating in the infrared. Effective nonlinearities of up to 10.7 pm/V and SHG conversion efficiencies of up to 66% (pulsed) have been obtained. Nevertheless, it has become clear that these QPM materials' potential as frequency converters does not primarily lie in the increased nonlinearity and efficiency, but rather in their flexibility in terms of output wavelengths, good power handling capability in terms of damage thresholds and thermal effects and finally in being available in large apertures. These properties have, for instance, allowed room-temperature generation of cw blue light exceeding 700 mW and pulse energies of up to 17 mJ in the infrared.

The results presented in this work clearly show that materials from the KTP family are well suited for being periodically poled into QPM nonlinear components for use in various applications. In comparison with PPLN they are particularly useful for short wavelength generation and for high power devices. Future work should focus on developing more homogenous material qualities and optimising poling and crystal preparation parameters, in order to further improve the reproducibility of the process.

Bibliography

1. M. Yamada, N. Nada, M. Saitoh, K. Watanabe, Appl. Phys. Lett. **62**, 435 (1993)
2. J. Webjörn, V. Pruneri, P. S. J. Russell, J. R. M. Barr, D. C. Hanna, Electron. Lett. **30**, 894 (1994)
3. L. E. Myers, R. C. Eckardt, M. M. Fejer, R. L. Byer, W. R. Bosenberg, J. W. Pierce, J. Opt. Soc. Amer. B **12**, 2102 (1995)
4. W. K. Burns, W. McElhanon, L. Goldberg, IEEE Photon. Technol. Lett. **6**, 252 (1994)
5. J. D. Bierlein, H. Vanherzeele, J. Opt. Soc. Am. B **6**, 622 (1989)
6. J. C. Jacco, SPIE **968** (Ceramics and inorganic crystals for optics, electro-optics and nonlinear conversion), 93 (1988)
7. M. Rottschalk, J-P. Ruschke, A. Rasch, J. opt. Commun. **17**, 34 (1996)
8. Y. V. Shaldin, R. Poprawski, Ferroelectrics **106**, 399 (1990)
9. R. C. Miller, Appl. Phys. Lett. **5**, 17 (1964)
10. A. Yariv, "Optical Electronics", 4:th edition, Saunders College Publishing
11. S. J. Brosnan, R. L. Byer, IEEE J. Quantum Electron. **QE15**, 415 (1979)
12. J. Yao, W. Sheng, W. Shi, J. Opt. Soc. Am. B **9**, 891 (1992)
13. J. A. Armstrong, N. Bloembergen, J. Ducuing, P. S. Pershan, Phys. Rev. **127**, 1918 (1962)
14. M. M. Fejer, G. A. Magel, D. H. Jundt, R. L. Byer, IEEE J. Quantum Electron. **28,** 2631 (1992)
15. L. E. Myers, W. R. Bosenberg, IEEE J. Quantum Electron. **33** 1663 (1997)
16. W. R. Bosenberg, A. Drobshoff, J. I. Alexander, L. E. Myers, R. L. Byer, Optics Lett. **21**, 1336 (1996)
17. P. E. Powers, T. J. Kulp, S. E. Bisson, Optics Lett. **23**, 168 (1998)
18. Aculight Corp. Bellwue, WA, USA
19. L. Goldberg, W. K. Burns, Appl. Phys. Lett. **67**, 2910 (1995)
20. G. Imeshev, M. Proctor, M. M. Fejer, Optics Lett. **23**, 673 (1998)
21. L. Becouarn, E. Lallier, D. Delacourt, CLEO-99, CThK33 (1999)
22. M. A. Arbore, O. Marco, M. M. Fejer, Optics Lett. **22**, 865 (1997)
23. G. Imeshev, A. Galvanauskas, M. A. Arbore, M. Proctor, D. Harter, M. M: Fejer, CLEO-98, CTuH1 (1998)
24. K. Mizuuchi, K. Yamamoto, M. Kato, H. Sato, IEEE J. Quantum Electron. **30**, 1596 (1994)
25. S. Helmfrid, G. Arvidsson, J. Webjörn, J. Opt. Soc. Am. B **10**, 222 (1992)
26. E. Lallier, L. Becouarn, M. Brévignon, J. Lehoux, CLEO-98, CFC4 (1998)
27. D. Zheng, L. A. Gordon, M. M: Fejer, R. L. Byer, K. L. Vodopyranov, CLEO-98, CFC5 (1998)
28. Y. H. Xue, N. B. Ming J. S. Zho, D. Feng, Chin. Phys. **4**, 554 (1984)

29. A. C. G. Nutt, V. Gopalan, M. C. Gupta, Appl. Phys. Lett. **60**, 2828 (1992)
30. M. C. Gupta, W. P. Risk, A. C. G: Nutt, S. D. Lau, Appl. Phys. Lett. **63**, 1167 (1993)
31. J. Webjörn, F. Laurell, G. Arvidsson, IEEE J. Lightwave Technol. **7**, 1597 (1989)
32. E. J. Lim, M. M. Fejer, R. L. Byer, W. J. Kozlovsky, Electron. Lett. **25**, 731 (1989)
33. A. Grisard, E. Lallier, G. Garry, P. Aubert, IEEE J. Quantum Electron. **33**, 1627 (1997)
34. K. Yamamoto, K. Mizuuchi, IEEE Photonics Technol. Lett. **4**, 435 (1992)
35. J. D. Bierlein, J. B. Brown, L. Conlin, M. G. Roelofs, F. Laurell, M. Pierrou, ECIO'97 8:th European Conf. on Int. Opt. Stockholm (1997)
36. W. P. Risk, G. M. Loiacono, Appl. Phys. Lett. **69**, 4157 (1996)
37. M. Houé, P. D. Townsend, J. Phys. D Appl. Phys. **28**, 1747 (1995)
38. G. D. Miller, R. G. Batchko, M. M. Fejer, R. L. Byer, SPIE 2700, 34 (1996)
39. L. K. Cheng, L. T. Cheng, J. Galperin, P. A. Morris Hotsenpiller,J. D. Bierlein, J. Crystal Growth **137**, 107 (1994)
40. G. M. Loiacono, D. N. Loiacono, R. A. Stolzenberger, J. Crystal Growth **131**,323 (1993)
41. P. F. Bordui, M. M. Fejer, *Inorganic crystals for nonlinear optical frequency conversion*, Annu. Rev. Mater. Sci. **23**, 321 (1993)
42. I. Camlibel, J. Appl. Phys. **40**, 1690 (1969)
43. J. D. Bierlein, F. Ahmed, Appl. Phys. Lett. **51**, 1322 (1987)
44. J. D.Bierlein, C. B. Arweiler, Appl. Phys. Lett. **49**, 917 (1986)
45. S. Furusawa, H Hayasi, Y. Ishibashi, A. Miyamoto, T. Sasaki, J. Phys. Soc. Jap. **62**, 183 (1993)
46. G. Hansson, FOA Linköping (Swedish Defense), Internal communication (1999)
47. T. Y. Fan, C. E. Huang, B. Q. Hu, R. C. Eckardt, Y. X. Fan, R. L. Byer, R. S. Feigelson, Appl. Opt. **26**, 2390 (1987)
48. V. A. Dyakov, V. V: Krasnikov, V.I: Pryalkin, M. S. Pshenichnikov, T. B. Razumikhina, V. S. Solomatin, A. I. Kholodnykh, Sov. J. Quantum Electron. **8**, 1059 (1988)
49. K. Kato, IEEE J. Quantum. electron. **27**, 1137 (1991)
50. D. L. Fenimore, K. L. Schepler, D. Zelmon, S. Kuck, U. B. Ramabadran, P. Von Richter, J. Opt. Soc. Am. B **13**, 1935 (1996)
51. V. G. Dmitriev, G. G. Gurzadyan, D. N. Nikogosyan, Handbook of Nonlinear Optical Crystals (Springer, Berlin, 1991)
52. K. Fradkin, A. Arie, A. Skliar, G. Rosenman, Appl. Phys. Lett. **74**, 914 (1999)
53. W. Wiechmann, S. Kubota, T. Fukui, H. Masuda, Optics Lett. **18**, 1208 (1993)
54. M. J. Missey, V. Domimie, L. E. Myers, R. C. Eckardt, Optics Lett. **23**, 664 (1998)
55. R. G. Batcjko, G. D. Miller, A. Alexandrevski, M. M: Fejer, R. L. Byer, CLEO-98, CTuD6 (1998)
56. M. Sato, T. Hatanaka, S. Izumi, T. Taniuchi, H. Ito, Appl. Opt. **38**, 2560 (1999)

57. L. Lefort, K. Puech, G. W. Ross, Y. P. Svirko, D. C. Hanna, Appl. Phys. Lett. **73**, 1610 (1998)
58. J.-P. Meyn, M. M. Fejer, Optics Lett. **22**, 1214 (1997)
59. A. Harada, Y. Nihei, Y. Okazaki, H. Hyuga, Optics Lett. **22**, 805 (1997)
60. Q. Chen, W. P. Risk, Electron. Lett. **30**, 1516 (1994)
61. W. P. Risk, S. D. Lau, Appl. Phys. Lett. **69**, 3999 (1996)
62. R. Stolzenberger, M. Scripsick, Conference on laser material crystal growth and nonlinear materials and devices, SPIE **3610**, 23 (1999)
63. G. Miller, *Periodically poled Lithium Niobate: Modeling, fabrication and nonlinear-optical performance*, PhD thesis, Stanford University (1998)
64. Q. Guan, J. Wang, W. Cui, J. Wei, Y. Liu,X. Yin, Cryst. Res. Technol. **33**, 821 (1998)
65. P. A. Morris, A. Ferretti, J. D. Bierlein, J. Cryst. Growth **109**, 367 (1991)
66. T. Hörlin, R. Bolt, Solid State Ionics **78**, 55 (1995)
67. G. Rosenman, A. Skliar, D. Eger, M. Oron, M. Katz, Appl. Phys. Lett. **73**, 3650 (1998)
68. A. Arie, G. Rosenman, V. Mahal, A. Skliar, M. Oron, M. Katz, D. Eger, Optics Commun. **142**, 265 (1997)
69. G. Rosenman, A. Skliar, Y. Findling, P. Urenski, A. Englander, P. A. Thomas, Z. W. Hu, J. Phys. D: Appl. Phys. **32**, L49 (1999)
70. M. G. Roelofs, P. A. Morris, J. D. Bierlein, J. Appl. Phys. **70**, 720 (1991)
71. K. Daneshvar, E. A. Giess, A. M. Bacon, D. G. Dawes, L. A. Gea, L. A. Boatner, Appl. Phys. Lett. **71**, 756 (1997)
72. T. Hörlin, Chem. Scr. **25**, 270 (1985)
73. F. Laurell, M. G. Roelofs, W. Bindloss, H. Hsiung, A. Suna, J. D. Bierlein, J. Appl. Phys. **71**, 4664 (1992)
74. W. J. Liu, S. S. Jiang, X. R. Huang, X. B. Hu, C. Z. Ge, Appl. Phys Lett. **68**, 25 (1996)
75. G. D. Boyd, D. A. Kleinman, J. Appl. Phys. **39**, 3596 (1968)
76. S. Helmfrid, G. Arvidsson, J. Opt. Soc. Am. B **8**, 2326 (1991)
77. I. Juwiler, A Arie, A. Skliar, G.Rosenman, Optics Lett. **24**, 1236 (1999)
78. G. Arvidsson, B. Jaskorzynska, *Proceedings of the International Conference on Materials for Non-linear and Electro-optics, Cambridge* **103**, 47 (1989)
79. S. D. Butterworth, S. Girard, D. C. Hanna, J. Opt. Soc. Am. B **12**, 2158 (1995)
80. S. A. Akhmanov, V. A. Vysloukh, A. S. Chirkin, *Optics of Femtosecond Laser Pulses* (American Institute of Physics, New york, 1992)
81. R. A. Baumgartner, R. L: Byer, IEEE J. Quantum Electron. **QE15**, 432 (1979)
82. A. J. Henderson, M. J. Padgett, F. G. Colville, J. Zhang, M. H. Dunn, Opt. Commun. **119**, 256 (1995)
83. M. Scheidt, B. Beier, R. Knappe, K. J. Boller, R. Wallenstein, J. Opt. Soc. Am. B **12**, 2087 (1995)

84. F. G. Colville, M. H. Dunn, M. Ebrahimzadeh, Optics Lett. **22**, 75 (1997)
85. D. T. Reid, M. Ebrahimzadeh, W. Sibbett, J. Opt. Soc. Am. B **12**, 2168 (1995)
86. L. R. Marshall, A.Kaz, J. Opt. Soc. Am. B **10**, 1730 (1993)
87. T. Schröder, K. J. Boller, A. Fix, R. Wallenstein, Appl. Phys. B **58**, 425 (1994)
88. E-mail correspondence between J. D. Bierlein and F. Laurell (1996)
89. A. M. Glass, Optical Engineering **17**, 470 (1978)
90. M. Taya, M. C. Bashaw, M. M. Fejer, Optics Lett. **21**, 857 (1996)
91. M. G. Roelofs, J. Appl. Phys. **65**, 4976 (1989)
92. B. Boulanger, M. M. Fejer, Appl. Phys. Lett. **65**, 2401 (1994)
93. G. M. Loiacono, D. N. Loiacono, J. Appl. Phys. **72**, 2705 (1992)
94. A. Alexandrovski, M. Fejer, G. Mitchell, CLEO-99, CFF5 (1999)